Virginia Commonwealth University
VCU Scholars Compass

Theses and Dissertations | Graduate School

2020

Disruption of the DREAM Complex Results in Cell Cycle Deregulation

Hayley C. Walston
Virginia Commonwealth University

Follow this and additional works at: https://scholarscompass.vcu.edu/etd

 Part of the Cell Biology Commons

© The Author

Downloaded from
https://scholarscompass.vcu.edu/etd/6382

This Thesis is brought to you for free and open access by the Graduate School at VCU Scholars Compass. It has been accepted for inclusion in Theses and Dissertations by an authorized administrator of VCU Scholars Compass. For more information, please contact libcompass@vcu.edu.

© Hayley C. Walston 2020
All Rights Reserved

DISRUPTION OF THE DREAM COMPLEX RESULTS IN CELL CYCLE DEREGULATION

A thesis submitted in partial fulfillment of the requirements of the degree of Master of Science at Virginia Commonwealth University.

By

Hayley C. Walston
B.A., University of Montana, Missoula MT

Thesis Director: Larisa Litovchick, M.D., Ph.D.
Associate Professor
Department of Internal Medicine
Division of Hematology, Oncology & Palliative Care

Virginia Commonwealth University
Richmond, VA
July 2020

ACKNOWLEDGEMENTS

First, I would like to thank my advisor, Dr. Larisa Litovchick, for the opportunity to work in her laboratory. Under her guidance, I have learned to always keep questioning and that sometimes there is more to experimental results than what meets the eye. She has been a source of support, inspiration, and advice during my graduate career. I appreciate her commitment to scientific integrity and hope to follow her example in the future. I also want to thank her for her calm and steadfast approach to the completion of my thesis work during the COVID-19 pandemic. She has guided me smoothly through the process in a time of great uncertainty and for that I am grateful.

I would also like to thank my advisory committee, Dr. Zheng Fu, Dr. Jennifer Koblinski, and Dr. Jolene Windle, for their advice, support, and guidance. I appreciate the flexibility they have all shown amid the COVID-19 pandemic. A special thank you goes to Dr. Windle for her role in creating both the *in vitro* and *in vivo* models used in this study.

I thank the other members of the Litovchick lab for all their help. Thank you to Supriya Joshi and Varsha Ananthapadmanabhan for always answering my many questions. Thank you to Sophia Gruszecki for making sure we had everything we needed and for assisting in experiments. And a big thank you to Fatumata Sesay for initially training me, continually helping me with all aspects of my project and for her unwavering support, both professionally and personally. This journey would not have been the same without her.

Finally, I want to thank my friends and family for all their encouragement. Whether near or far, they have been with me on this journey and it would not have been the same without them. I want to especially thank my parents; whose love and support made my dream possible.

TABLE OF CONTENTS

LIST OF FIGURES

LIST OF ABBREVIATIONS

ATCC	American Type Culture Collection
BSA	Bovine Serum Albumin
CDK	Cyclin Dependent Kinase
ChIP	Chromatin Immunoprecipitation
DMEM	Dulbecco's Modified Eagle Medium
DNA	Deoxyribonucleic Acid
DP	Dimerization Partner
DREAM	DP, Rb-like, E2F, And MuvB
dREAM	*Drosophila* RBF, E2F2, And Myb
DYRK1A	Dual Specificity Tyrosine Phosphorylation Regulated Kinase 1A
FOXM1	Forkhead Box M1
GFP	Green Fluorescent Protein
HPV	Human Papilloma Virus
HRP	Horseradish Peroxidase
IP	Immunoprecipitation
MEF	Mouse Embryonic Fibroblast
MudPIT	Multidimensional Protein Identification Technology
Muv	Multi-vulva phenotype
PBS	Phosphate Buffered Saline
PP1	Protein Phosphatase 1

Rb	Retinoblastoma
RT	Room Temperature
SA β-gal	Senescence Associated Beta Galactosidase
S20	Serine 20
TBS	Tris Buffered Saline
VCM	Virus Conditioned Medium
β-ME	Beta-Mercaptoethanol

ABSTRACT

The Dimerization Partner, Rb-like, E2F, And MuvB (DREAM) complex was identified in humans due to homology of the genes involved in the *D. melanogaster* dREAM complex. It assembles during cellular arrest, or G0, to function as a transcriptional repressor of cell cycle genes. It is known that phosphorylation of LIN52 at serine 28 is necessary for the critical DREAM forming interaction between LIN52 and the pocket protein p130. Our laboratory has previously shown that gene editing of LIN52 to replace serine 28 with alanine (S28A) prevents phosphorylation by the kinase DYRK1A and inhibits DREAM formation. Here we have confirmed this model and used it to investigate cell cycle regulation in the absence of DREAM. Our approach included both *in vitro* and *in vivo* methods using genetically engineered S28A Lin52 mice and immortalized MEFs. We have shown that DREAM loss deregulates the cell cycle, increasing proliferation and displaying reduced oncogenic Ras induced senescence. Restoration of DREAM rescues these phenotypes to a degree. While characterizing S28A mice we observed a general decrease in body weight and shortened lifespan in males. Overall, we have demonstrated the role of DREAM in control of cell cycle exit and how loss of this complex leads to rapid proliferation, potentially aiding in cellular transformation.

CHAPTER ONE: INTRODUCTION

1.1 The Retinoblastoma Family of Proteins

The retinoblastoma gene *RB1*, originally identified as a susceptibility gene for the cancer retinoblastoma (Friend et al., 1986, Lee et al., 1987), is known ubiquitously as a potent tumor suppressor. *RB1* and its homologs *RBL1* and *RBL2*, encoding for gene products Rb, p107 and p130, respectively, make up the retinoblastoma family. They are also known as pocket proteins, named for their conserved pocket shaped domain. These proteins share sequence homology and similar structure, but also contain features unique to themselves. As a group they act as negative regulators of the cell cycle by binding and blocking E2F transcription factors (Hiebert et al., 1992). The pocket proteins cooperate to complete this task by performing both redundant and unique functions.

1.2 Pocket Protein Structure

The most highly conserved feature of this protein family is a protein binding groove called the pocket domain (reviewed in Henley and Dick, 2012). This domain interacts with the LXCXE motif of other cellular proteins, including some oncogenic viral proteins (Dick, 2007). The pocket contains two domains, the A and B boxes, with a spacer region in between (Figure 1A). Within the B box is the LXCXE interacting site, which allows Rb family proteins to carry out some of their most critical functions, such as E2F binding (Lee et al., 1998). The pocket domain and C terminal region are both required for the binding of E2F transcription factors to any pocket protein (Qin et al., 1992). While the retinoblastoma family proteins are structurally similar, there

are a few noteworthy distinctions between them. For instance, Rb contains a specific E2F1 binding site not seen in the other two proteins (Rubin et al., 2005). Rb also has a docking site within the C terminus that binds competitively to cyclin/CDK complexes and protein phosphatase 1 (PP1). The cyclin/CDK binding domain of p107 and p130 is located within the spacer region. Another important difference is the presence of a CDK inhibiting region in the N terminus of p107 and p130 that Rb lacks (Woo et al., 1997). These two proteins also contain an insertion in the B domain that, in the case of p130, serves as a regulatory phosphorylation site. The structural comparison of these proteins relates to the functional similarities and differences between them and will be discussed later.

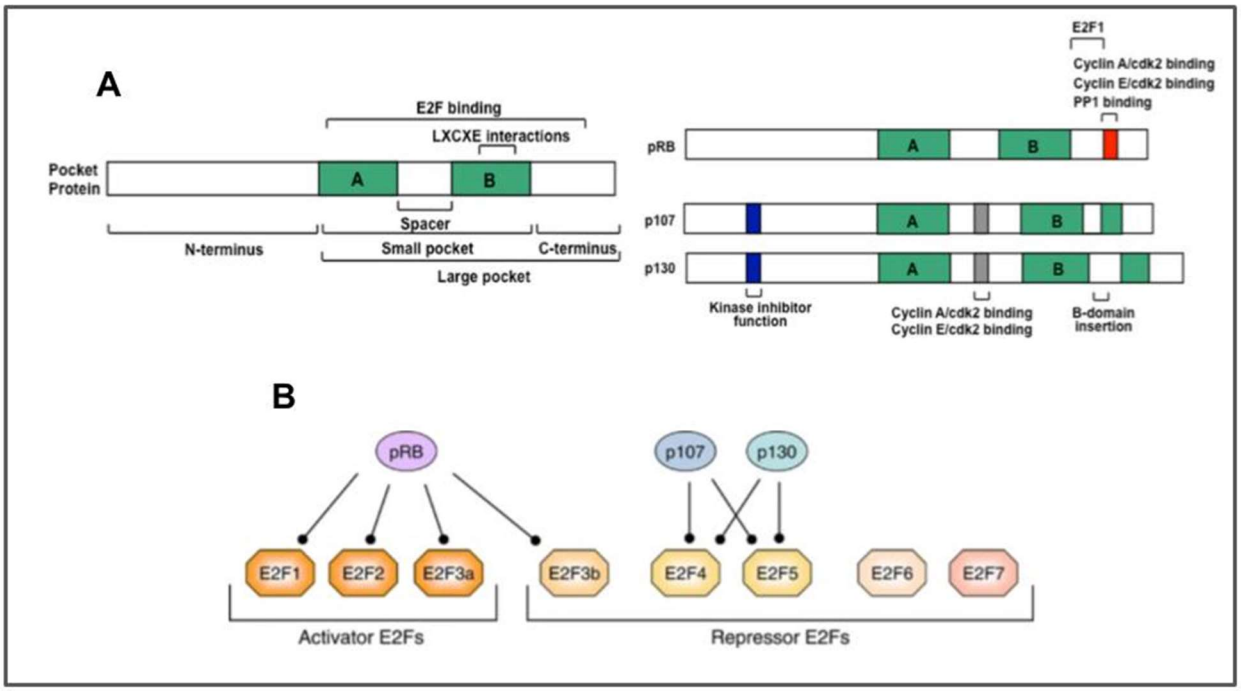

Figure 1. Structure and E2F binding specificity of the retinoblastoma protein family. A) General features of pocket proteins include an E2F binding domain, an LXCXE interacting site, and a cyclin/CDK binding region. Unique to p107/p130 are a kinase inhibitor domain and enlarged spacer region (adapted from Henley and Dick, 2012). B) Preferential binding of pocket proteins and E2F transcription factors (adapted from Cobrinik, 2005).

1.3 Pocket Protein Regulation of E2F Transcription Factors

The E2F family is made up of nine E2F proteins (E2F1, E2F2, E2F3a, E2F3b, E2F4, E2F5, E2F6, E2F7, and E2F8) and three heterodimeric binding partners (DP1, DP2, and DP3)

(DeGregori, 2002). E2F proteins 1-6 contain a dimerization domain necessary for interaction with DP1, DP2, or DP3 to facilitate binding to the E2F consensus site in promoters of target genes (Dyson, 1998). The E2F family is divided into either ‘activators’ or ‘repressors’, determined by their effect on target gene expression. The activators (E2F1, E2F2, and E2F3a) activate transcription of the genes necessary for the G1/S transition of the cell cycle, such as those required for DNA synthesis (Wells et al., 2000). On the other hand, the repressors E2F4 and E2F5 work to inhibit transcription of these genes and induce cell cycle exit into G0 (Gaubatz et al., 2000). E2F3b, E2F6, E2F7, and E2F8 are also known as transcriptional repressors, however they are not regulated by pocket proteins. Only E2F1-5 contain pocket protein interacting sites through which Rb family proteins can bind and inhibit transcriptional activation by blocking the transactivation domain (Rubin et al., 2005). Pocket proteins do not bind with equal affinity to these E2F proteins (Figure 1B). Rb binds preferentially to the activators (E2F1, E2F2, and E2F3) while p130 and p107 preferentially bind to the repressors (E2F4 and E2F5) (Trimarchi and Lees, 2002).

1.4 Cell Cycle Progression and Exit

The cell cycle is a complex and highly regulated process involved in cellular proliferation, differentiation, deoxyribonucleic acid (DNA) repair, and development. It is composed of four phases: G1 (gap phase 1), S (synthesis phase), G2 (gap phase 2), and the M phase (mitosis) (Figure 2A) (Cobrinik, 2005). The gap phases allow the cell to grow and prepare for the replication of the genome during S phase and division into daughter cells during M phase. The G1/S and G2/M transitions are referred to as the G1 and G2 checkpoints, respectively. These checkpoints serve to halt the cell cycle if certain conditions are not met. A cell will not pass through the G1 checkpoint to S phase unless growth signals are present and lead to the transcription of DNA synthesis genes. At the G2 checkpoint, the genome is assessed for replication errors to prevent production of mutated daughter cells. If none are found the cell will

proceed into mitosis. After division, a cell may choose not to re-enter the cell cycle and go into a resting stage referred to as G0, or quiescence (Malumbres and Baracid, 2001, Schafer, 1998). Cells enter G0 in response to antimitotic signals or lack of mitotic signals, such as the absence of growth factors. These signals stop the cell from passing the G1 checkpoint and instead lead to a temporary arrest of the cycle. Because they inhibit E2F target gene expression, pocket proteins are critical for G0 arrest of the cell cycle.

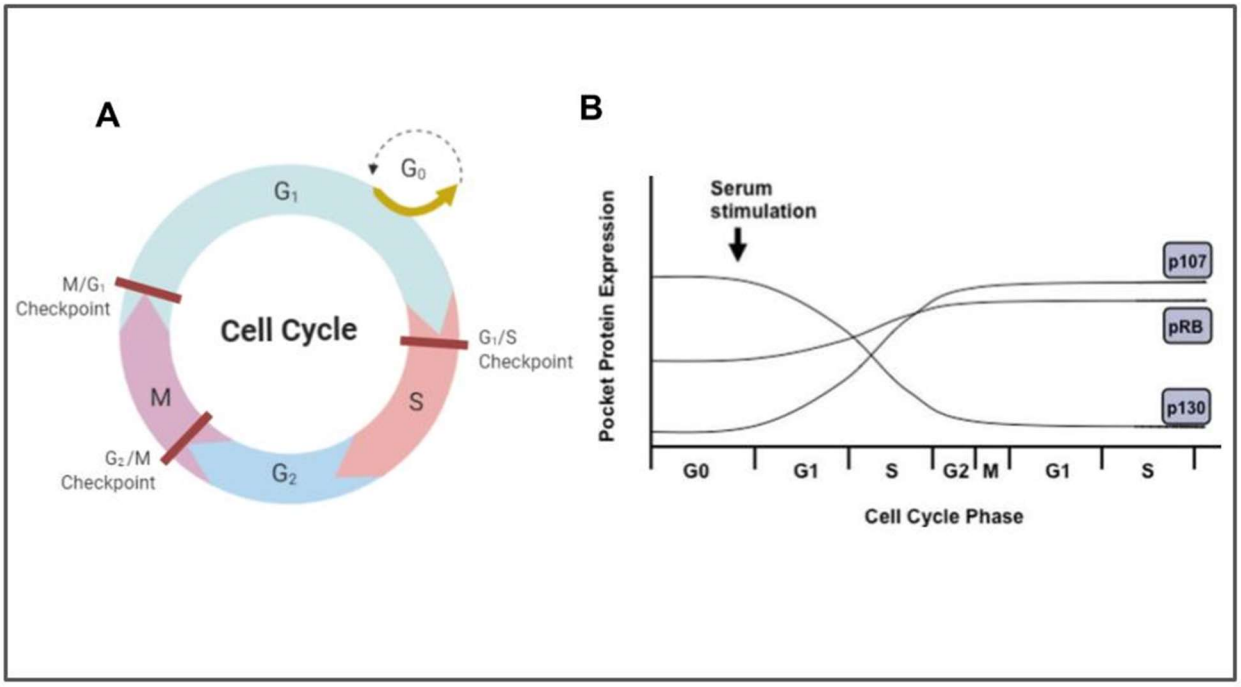

Figure 2. The cell cycle and corresponding pocket protein levels. A) Phases and checkpoints of the cell cycle (image created in BioRender.com). B) Cell cycle-dependent changes in pocket protein expression levels (adapted from Henley and Dick, 2012).

1.5 Cell Cycle Regulation

The cell cycle is tightly regulated by proteins called cyclins, whose expression levels vary with the cell cycle. Cyclins bind and activate cyclin dependent kinases (CDKs). These kinases then act on pocket proteins, leaving them hyperphosphorylated and causing them to release E2F transcription factors (reviewed in Cobrinik, 2005). During G0 and early G1 the pocket proteins are hypophosphorylated and can bind their respective E2F family members. p130 is the most highly expressed pocket protein during G0 and works in complex with E2F4/5

to bind and repress E2F target genes. Rb is found sequestering E2F1-3 and levels of p107 are very low at this point (Figure 3) (reviewed in Henley and Dick, 2012). As the cell receives mitotic signals and moves into G1, transcription of cyclin D is triggered. The cyclin D-CDK4/6 complex forms and begins phosphorylating pocket proteins. Release of E2F transcription factors leads to the transcription of the gene for cyclin E, which is E2F responsive. cyclin E complexes with CDK2 and further phosphorylates Rb family proteins, increasing DNA synthesis gene expression and pushing the cell into S phase. p130 levels drop in mid G1, while p107 increases and replaces p130 at E2F promoters (Takahashi et al., 2000). Throughout G1 and S, p130 levels continue decreasing and remain low for the rest of the cycle, while p107 levels remain high. Rb is expressed fairly consistently through the cycle, with a small increase during G1 and S (Figure 2B).

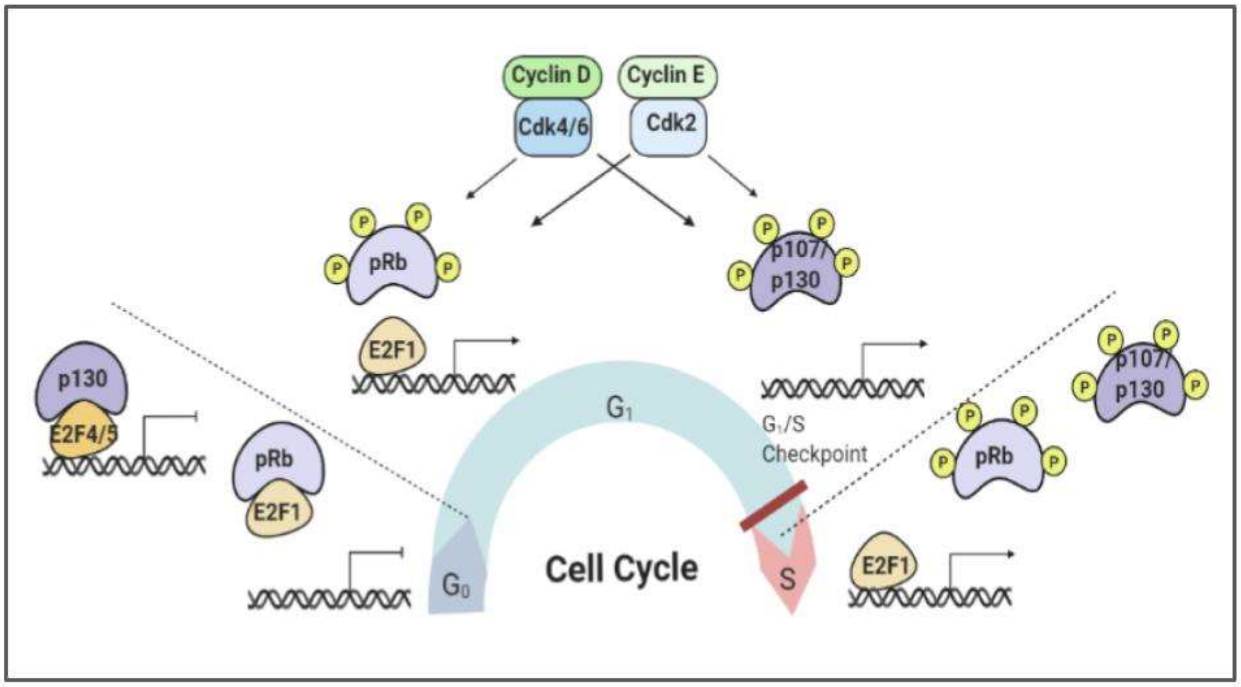

Figure 3. Regulation of the G0/G1/S transitions. The activity of cyclin/CDK complexes, pocket proteins, E2F transcription factors and E2F target genes during the G0/G1 and G1/S transitions (image created in BioRender.com).

1.6 Unique and Redundant Functions of the Rb Family Proteins

While the three pocket proteins work together to repress E2F target genes in G0/G1, they each have unique functions as well. For example, p130 is the most prominent pocket protein during G0 and complexes with E2F4 to perform the bulk of E2F target repression in this phase. Coinciding with this, p130 is most abundant in quiescent cells, p107 in proliferating cells, and Rb is present in both (Classon and Dyson, 2001). p107 can replace p130 and repress the same genes, but many of these do not overlap with those repressed by Rb. A study of gene expression in mouse embryonic fibroblasts (MEFs) with knockout of Rb, p107, p130, or both p107 and p130, found that E2F target genes are deregulated in cells lacking Rb or p107 and p130. However, the deregulated genes identified were not the same between the two groups (Hurford et al., 1997). There was also no difference between p107 and p130 knockouts, indicating redundancy in their targets. Another shared ability of p107 and p130 is inhibition of cyclin A-CDK2 and cyclin E-CDK2 kinases (Woo et al., 1997). Rb lacks a kinase inhibitor domain but regulates CDKs by stabilizing the cyclin dependent kinase inhibitor (CKI) p27 (Ji et al., 2004).

1.7 The DREAM Complex

Another distinction between the p107/p130 pair and Rb is their role in an evolutionarily conserved cell cycle regulatory complex. Studies in *Drosophila melanogaster* and *Caenorhabditis elegans* first identified multi-subunit DNA binding complexes containing Rb proteins, which later led to a discovery of related regulatory complexes in humans, referred to as the DP, Rb-like, E2F, and MuvB (DREAM) complex and the Myb-MuvB (MMB) complex. First, the *D. melanogaster* homolog of the human transcription factor Myb, dMyb, was found to bind four other proteins at regulatory DNA elements in a site specific manner and to play a role in gene expression in follicle cells (Beall et al., 2002). The associated factors included chromatin assembly factor 1, p55 subunit (CAF1p55), Mip40, Mip120, and Mip130 and was referred to as

the Myb complex. Another study identified regulatory complexes when purifying the fly Rb homologs, RBF1 and RBF2, from *Drosophila* embryo extracts. These consisted of dDP, RBF1 or RBF2, dE2F, and dMyb, as well as Mip40, Mip120, Mip130, and CAF1p55. This complex was termed *Drosophila* RBF, E2F, and Myb, or dREAM and was localized to transcriptionally repressed chromatin (Korenjak et al., 2004). Interestingly, all the dREAM components except Myb are related to members of synMuv class B, a group of genes involved in the vulval development of *Caenorhabditis elegans* (reviewed in Fay and Han, 2000). synMuv class B and class A genes redundantly inhibit the Ras/MAPK signaling pathway, leading to differentiation of the *C. elegans* vulva. When class B genes are inactivated in combination with class A, the multi-vulva phenotype (Muv) results due to an increase in vulva cell fate induction. synMuv B genes encoding proteins related to dREAM components include *lin-35* (RBF), *dpl-1* (dDP), *efl-1* (dE2F), *lin-9* (Mip130), and *lin-53* (CAF1p55) (Ceol and Horvitz, 2004). *C. elegans* proteins LIN-35, LIN-9, LIN-37 (MIP40), LIN-52, LIN-54 (MIP120), and DPL-1 were later found to form a dREAM like complex, referred to as DPl-Rb-MuvB, or DRM (Harrison et al., 2006). It was later shown that MMB/dREAM acts as both transcriptional repressor and activator of different subsets of genes in *Drosophila* (Georlette et al., 2007). Human homologs of the Mip40, Mip120, and Mip130 dREAM subunits were identified, and recombinant forms were shown to interact with GST-pRB fusion proteins (Korenjack et al., 2004). Multidimensional protein identification technology (MudPIT) proteomic analysis was later used to identify proteins associated with human homologs LIN9 (Mip130), LIN37 (Mip40), and LIN54 (Mip120) in human cells. This resulted in the discovery that LIN9, LIN37, and LIN54 bind to each other, along with other MuvB proteins LIN52, and RBBP4 (CAF1p55) to form a MuvB complex that can exist on its own or bound to p130, E2F4/5, and DP1/2 together (Litovchick et al., 2007). Co-immunoprecipitation experiments confirmed these interactions and revealed that human B-Myb precipitated with LIN9, LIN37, and LIN54, but not p130, indicating the MuvB core forms distinct complexes with these two proteins. Out of the three pocket proteins, p130 and p107 both coprecipitated all of

the MuvB proteins, but Rb did not. When containing p107/p130 and associated proteins, this complex became known as the human DP, Rb-like, E2F and MuvB (DREAM) complex (Figure 4) (Litovchick et al., 2007). The MuvB core bound to B-Myb is now referred to as the Myb-MuvB (MMB) complex.

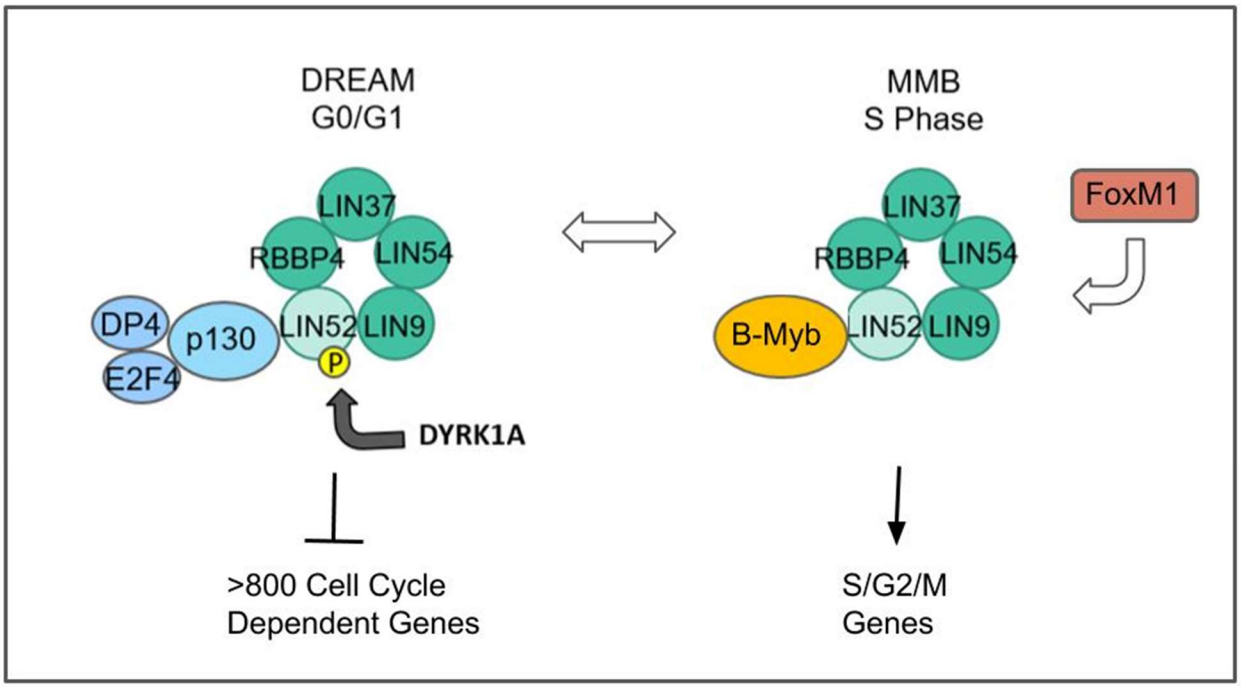

Figure 4. Composition and formation of the DREAM/MMB complexes. The DREAM complex consists of the MuvB core bound to p107/p130, E2F4/5, and DP1/2. Phosphorylation of LIN52 by the DYRK1A kinase is necessary for DREAM assembly (see section 1.9) (Litovchick et al., 2011). MMB consists of the MuvB core bound to B-Myb. The transcription factor FOXM1 interacts with MMB after S phase to promote transcription of G2 and M phase genes (see section 1.8) (Sadasivam et al., 2012).

1.8 The Function and Regulation of Mammalian DREAM/MMB

When investigating the function of DREAM, it was important to consider the known role of p130/E2F4 complexes in transcriptional repression of E2F target genes during G0 and the transcriptional activation role of B-Myb in S phase. Indeed, proteomic and immunoprecipitation analyses revealed an abundance of reciprocal binding between DREAM subunits and p130 in G0, whereas the still intact MuvB core bound only B-Myb in S phase (Litovchick et al., 2007, Pilkinton et al., 2007). These findings suggested that DREAM forms during G0 and the MuvB

core disassociates from p130/E2F4 and binds B-Myb to form the MMB complex in S phase (Figure 4). Tracking the levels of p107/p130/E2F4 bound to MuvB with the levels of cyclin D/CDK4 expression, along with evidence that hyperphosphorylated p130 does not co-precipitate the MuvB proteins, further demonstrated the cell cycle dependent formation of DREAM (Pilkinton et al., 2007). The timing and function of p130 expression, along with its interaction with MuvB proteins during quiescence suggested that DREAM may also bind E2F target promoters. Indeed, chromatin immunoprecipitation (ChiP) and microarray analysis of the promoters commonly bound by DREAM subunits p130, E2F4, LIN9 and LIN54 revealed significant enrichment of genes with E2F binding sites, such as *E2F1, RBL1*, and *CDC6*. These were validated using ChIP followed by polymerase chain reaction (Litovchick et al., 2007). Binding of these promoters also coincided with reduced gene expression, whereas knockdown of select DREAM targets led to a G0 specific increase in expression of tested target genes. In summation, DREAM forms in G0 to repress cell cycle genes and maintain the cell in a quiescent state.

B-Myb, (encoded by the *MYBL2* gene) a component of MMB, is itself an E2F regulated gene whose expression is initiated by DREAM disassociation and re-entry into the cell cycle. B-Myb is an important activator of G2/M related genes and interacts with the MuvB core in S phase (Zhu et al., 2004, Sadasivam et al., 2012). A significant overlap of target promoters between B-Myb and MuvB was identified with genome wide ChIP-sequencing analysis, and included many late cell cycle genes. The MuvB core and B-Myb also required each other to bind these target promoters (Sadasivam et al., 2012). B-Myb binding of target promoters lessens through G2 and M, coinciding with B-Myb expression levels. However, LIN54 is present on promoters in G2, indicating the MuvB core remains bound after B-Myb disassociates. B-Myb is known to be phosphorylated in S phase and, through proteasome inhibition and immunoprecipitation experiments, it was found that this phosphorylation did not cause B-Myb to separate from MuvB, but lead to its degradation (Sadasivam et al., 2012). Interestingly, this

degradation preceded the peak expression of some late cell cycle genes, suggesting the existence of a transcriptional coregulator. Forkhead box protein M1 (FoxM1) was identified to be this coregulator through a motif analysis of the B-Myb/MuvB bound genomic regions. Furthermore, FoxM1 was shown to interact with MuvB proteins at the promoters of late cell cycle genes during G2 and M. B-Myb and FoxM1 can co-occupy these promoters and, in fact, B-Myb and LIN9 are required for FoxM1 recruitment to promoters. FoxM1, but not B-Myb, is present on these promoters when the genes become fully active, indicating FoxM1 is recruited by B-Myb and the MuvB core to promote gene expression in G2/M (Sadasivam et al., 2012).

It is now clear that the MuvB core has multiple roles in regulating the cell cycle. During G0, it binds with p130/E2F4/DP1 to promoters of early cell cycle genes and reduces expression. Once a new cycle begins, p130 becomes hyperphosphorylated and inactivated by cyclin/CDK complexes. With release of p130/E2F4 complexes from gene promoters, B-Myb expression is induced. The now available MuvB complex binds B-Myb, forming the MMB complex and activating genes necessary for the synthesis of DNA. Later in S phase, MMB recruits FoxM1 to late cell cycle promoters prior to the degradation of B-Myb and the expression of G2/M genes. In this way, the MuvB core aids in the regulation of cell cycle progression.

1.9 Assembly of the Mammalian DREAM/MMB Complex

The assembly of DREAM/MMB was investigated with an immunoprecipitation and proteomic approach to identify and catalog the status of phosphorylation sites within each subunit when co-precipitated. The serine 28 (S28) site of LIN52 was exclusively found in the phosphorylated state when co-immunoprecipitated with p130 but was present in both forms when precipitated with B-Myb (Litovchick et al., 2011). A mutated form of LIN52 in which alanine replaced serine 28 (S28A) was unable to bind p130, demonstrating the necessity of LIN52 S28 phosphorylation for DREAM formation. This phosphorylation is not required for MMB assembly, as the S28A mutation did not change the ability of LIN52 to bind B-Myb, LIN37, or Lin9. The

kinase responsible for this phosphorylation, whose identity was discovered through a search of MudPIT proteomic data, is Dual-specificity tyrosine-(Y)-phosphorylation Regulated Kinase 1A (DYRK1A) (Figure 4) (Litovchick et al., 2011). DYRK1A is a member of the DYRK family of kinases, which catalyze the phosphorylation of serine/threonine residues of protein substrates and are involved in cell cycle regulation (Becker et al., 1998). DYRK1A can recognize the RX(X)(S/T)P consensus motif to target substrates and the region surrounding LIN52 S28 is highly similar to this (Himpel et al., 2000, Litovchick et al., 2011). *In vitro* kinase assays confirmed the ability of DYRK1A to phosphorylate the S28 site of LIN52 whereas limiting the kinase, whether by depletion or drug inhibition, reduced phosphorylated LIN52 levels. Loss of DYRK1A function also decreased LIN52/p130 interactions, increased the binding between LIN52 and B-Myb, and induced DNA synthesis in serum starved cells (Litovchick et al., 2011). Taken together this demonstrates the requirement of DYRK1A phosphorylation of LIN52 for the formation of DREAM and entry into quiescence.

The need for LIN52 phosphorylation as a prerequisite for binding between p130/E2F4/DP1 and the MuvB core indicated these two groups are joined by a specific interaction between p130 and LIN52. This was confirmed when purified, recombinant p130 and phosphorylated LIN52 coprecipitated in a binding experiment (Guiley et al., 2015). Removal of phosphates from p130 with λ phosphatase stabilized the interaction, suggesting that well-characterized pocket protein regulation by hyperphosphorylation also applies to DREAM. Therefore, DREAM formation was established as a direct interaction between LIN52 and p107/p130, dependent on S28 site phosphorylation of the former and hypophosphorylation of the latter.

1.10 DREAM Disruption: Mechanisms, Consequences, and Cancer

There are many ways in which DREAM could be inactivated by alterations in the signaling pathways that affect its formation. For instance, loss of the DYRK1A kinase has been

shown to disrupt DREAM, reduce the ability of cells to arrest the cell cycle, and increase proliferation (Litovchick et al., 2011). DYRK1A is frequently altered in cancers, over 80% of cases in some types (Figure 5A, TCGA data). Besides freeing up the MuvB core, DREAM disruption increases transcription of *MYBL2*, the gene encoding B-Myb. Deregulation of B-Myb can further shift the balance from DREAM formation to MMB formation (Figure 6). It was recently shown that B-Myb overexpression inhibits DREAM formation in human cells (Iness et al., 2017). Importantly, B-Myb is often found to be upregulated in tumors and correlates with poor patient outcome (Figure 5B) (reviewed in Musa et al., 2017, Iness, 2018).

Increase in cyclin/CDK activity could also reduce DREAM by p130 hyperphosphorylation and inactivation (Figure 6). DREAM disassembly has been correlated to the high levels of Cdk4 activity present during the G1/S transition, which supports the idea that DREAM can be disrupted by an excess of CDKs (Pilkinton et al., 2007). In fact, deregulation of cyclins, CDKs, and CDK inhibitors are found in a variety of human cancers (reviewed in Malumbres and Barbacid et al., 2009).

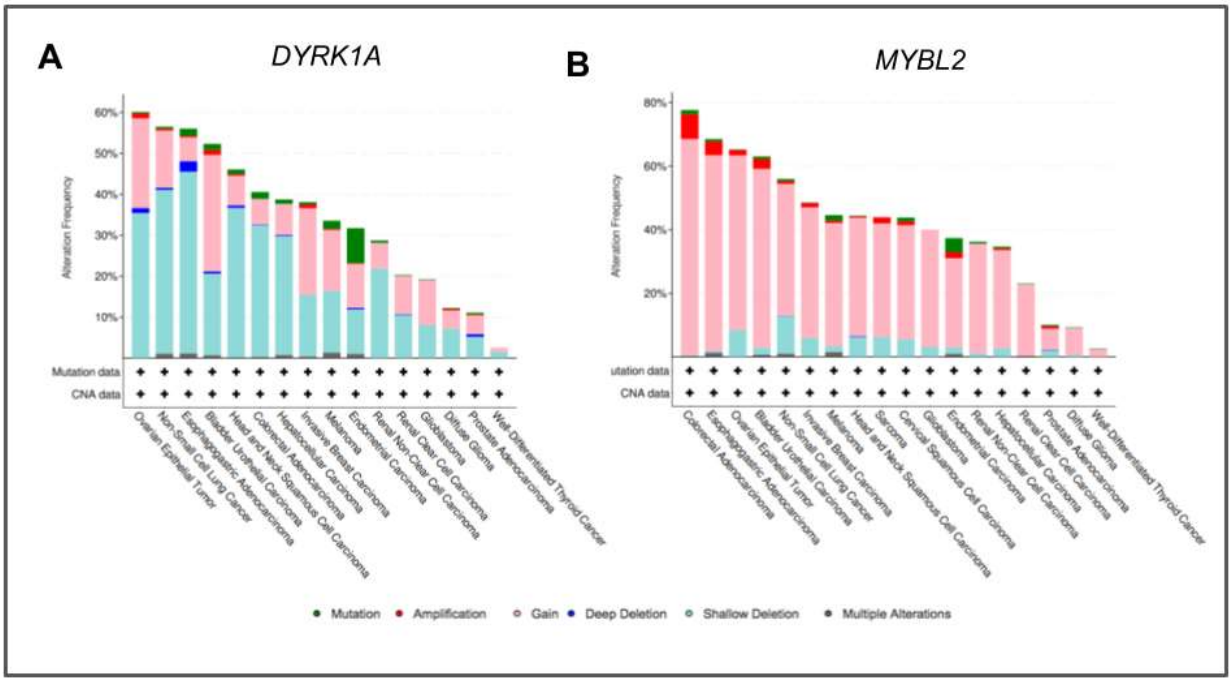

Figure 5. *DYRK1A* and *MYBL2* in cancer. Genetic alterations of *DYRK1A* (A) and *MYBL2* (B) across different types of cancer were summarized using cBio.org online tool and the TCGA PanCancer dataset. All studies with sample number of 250 and higher were included. Pink and red color indicates gene copy number gains and amplifications, respectively. Light and dark blue colors correspond to shallow or deep deletions, and green color indicates mutations. (Figure provided by L. Litovchick).

1.11 DREAM Interruption by Viral Oncoproteins

The study of small DNA tumor viruses began with the observation that polyoma virus, SV40, and common human adenoviruses caused tumors to form in a variety of animals (reviewed in DeCaprio, 2009). A search for viral oncogenes and host cell protein interactors began, encouraged by the contamination of polio vaccine by SV40. The discovery of the retinoblastoma protein during this time allowed scientists to identify Rb as a binding partner of adenovirus E1A, SV40 LT, and human papilloma virus (HPV) E7 viral protein products (Whyte et al., 1988, DeCaprio et al., 1988, Dyson et al., 1989). Mutations of the highly conserved LXCXE motif identified in viral proteins prohibited Rb binding, indicating an intact motif is required for interaction of these proteins with Rb. Both p107 and p130 were discovered because they interact with E1A in the same manner. It was later found that E7, E1A, and LT all target

pocket proteins through the LXCXE motif, resulting in relief of E2F target gene repression (reviewed in Helt & Galloway, 2003). HPV E7, which is expressed in almost all cervical cancers, has been specifically shown to inhibit DREAM through interaction with p130 in HPV-positive cervical carcinoma cells (Rashid et al., 2011).

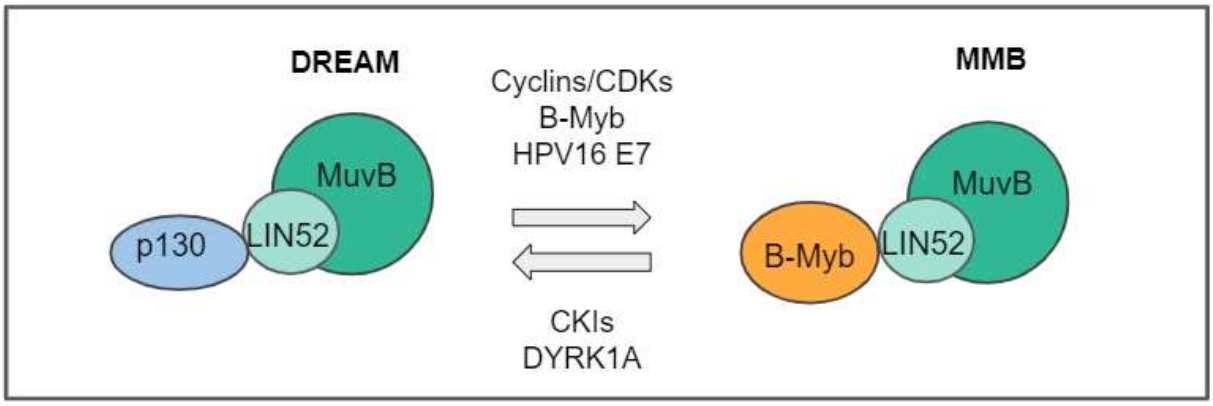

Figure 6. Mechanisms regulating DREAM formation. Different cellular alterations can cause deregulated DREAM assembly, resulting in a shift of balance in DREAM and MMB complexes.

1.12 *In Vivo* Models of Pocket Protein and DREAM Loss

Study of the three Rb family proteins *in vivo* has been difficult due to the lethality of pocket protein gene loss. Early studies in mice found homozygous loss of Rb to be embryonic lethal, demonstrating its importance in development (Clarke et al., 1992, Lee at al., 1992, Jacks et al., 1992). Homozygous p107 mutants are viable and display normal viability up to 24 months of age with no pathologic abnormalities (Lee et al., 1996). $Rb^{+/-};p107^{-/-}$ mice have severe growth delays in the first weeks of life, weighing half as much as their littermates. Only a quarter of these mice survived past 3 weeks and reached 70% - 90% of their normal weight by 3 months. Similar to p107 mutants, p130 null mice are viable and display minimal developmental defects (Cobrinik et al., 1996). Within this model, p107 was shown to replace p130 as a major E2F interactor, which is now known to include involvement in the formation of DREAM. Because of this, both p107 and p130 must be lost to inhibit DREAM by pocket protein depletion. However, double p130, p107 homozygous knockout mice die during birth or shortly after (Cobrinik et al.,

1996). Interestingly, these pups were smaller than their littermates, with severely shortened limbs due to reduced bone deposition.

To combat the lethality issue, one group successfully created a mutant form of p107 in which the LXCXE interacting site is unable to interact with MuvB subunits LIN9, LIN37, and LIN54. This allele was referred to as $p107^{\Delta D}$ (Forristal et al., 2014). These mice were bred with p130 knockout mice to create $p107^{\Delta D/\Delta D}$; $p130^{-/-}$ mouse embryos. Immunoprecipitation of LIN37 from embryonic fibroblasts confirmed the loss of interaction between p107 and LIN37 and expression of DREAM target genes was substantially higher in $p107^{\Delta D/\Delta D}$; $p130^{-/-}$ cells compared to $p107^{\Delta D/\Delta D}$; $p130^{+/+}$ cells. However, most double homozygous mutants were not viable, with a maximum survival time of 1.5 days post birth. Comparing this to the fairly normal phenotypes of p130-null and p107-null mice suggests a more DREAM-specific role in development, although the loss of non-DREAM related functions of p130 in this model should be considered.

Other models have targeted the MuvB core instead of pocket proteins to study the physiological role of DREAM. One such model includes a Lin9 knockout strain generated by inserting a gene trap vector into the Lin9 locus (Reichert et al., 2010). This insertion leads to a truncated protein that is expected to be nonfunctional. However, there were no homozygous $Lin9^{-/-}$ offspring obtained from heterozygous $Lin9^{+/-}$ mice crossings, while heterozygous offspring displayed normal development and fertility. Therefore, it was determined that loss of LIN9 is embryonic lethal in mice. Genotype analysis revealed that Lin9-null embryos only survived between 3.5 and 7.5 embryonic days, preventing researchers from performing any long-term phenotypic study. They then created a conditional Lin9 knockout strain instead, by inserting LoxP sites on either side of exon 7 and crossing these with a Cre-recombinase “delete” strain. Again, this allele proved to be embryonic lethal at homozygosity. Mouse embryonic fibroblasts obtained from these mice displayed mitotic defects and dramatically decreased proliferation, due to disruption of the MMB complex resulting from loss of LIN9 that has been shown to be the main structural component of MuvB (Schmit et al., 2007, Guiley et al., 2018). This model, while

useful in uncovering the importance of LIN9 and MMB complex in early embryonic development, does not provide an opportunity to characterize the role of DREAM *in vivo*.

Although previous models have provided valuable information, there is a need for an *in vivo* model of DREAM loss in which animal lifespan is extended. This would allow for a range of *in vivo* methods to investigate the effects of DREAM inhibition across the lifespan, such as phenotypic characterization and histological studies. Also important is the specificity of the model, given the role of DREAM subunits in different protein-protein interactions outside of this complex. A model specifically targeting DREAM formation would provide an opportunity to explore the physiological role of this complex without the complication of confounding effects resulting from loss of any of its multi-functional subunits.

CHAPTER TWO: MATERIALS AND METHODS

2.1 Animal studies

All animal studies and care were performed under the guidelines of the Virginia Commonwealth University Institutional Animal Care and Use Committee (IACUC), in accordance with the principles and procedures outlined in the National Research Council "Guide for the Care and Use of Laboratory Animals". Animals were housed in individually ventilated cages in a barrier vivarium with regular testing for known mouse viruses and parasites and most bacteria (including helicobacter), under a 12 hr light/12 hr dark light schedule, and were fed standard mouse chow (irradiated Teklad LM-485 diet) and autoclaved water *ad libitum*. (Methods provided by VCU Transgenic/Knockout Mouse Core).

2.2 Generation of Lin52 S28A Knockin Mice

A CRISPR/Cas9 approach was employed to generate Lin52 S28A knockin mice, using methods modified from Jacobi et al., 2017. A guide RNA protospacer sequence was selected using a combination of the MIT CRISPR Design Tool developed by Hsu et al., 2013 (tool no longer available), and the Broad Institute sgRNA design tool developed by Doench et al., 2014 (see Figure 7B for the protospacer sequence). This sequence was used to generate an Alt-R crRNA, which was then annealed to the Alt-R tracrRNA (both from Integrated DNA Technologies, IDT) to generate the functional guide RNA. Homology-directed repair at the Cas9 cleavage site utilized a 200-base, sense-strand, single-stranded oligodeoxynucleotide (ssODN) spanning *Lin52* exon 2 (Fig. 7A). The ssODN contained a total of three base substitutions that: (1) generated a serine-

to-alanine mutation at codon 28, (2) created an AluI site for screening purposes, and (3) destroyed the Cas9 PAM sequence to prevent retargeting. A mix containing 40 ng/µl Cas9 protein (IDT), 20 ng/µl annealed cr/tracrRNA (preincubated with the Cas9 protein at R.T. for 10 min), and 20 ng/µl ssODN (IDT) was microinjected into fertilized C57BL/6J mouse eggs by the VCU Transgenic/Knockout Mouse Core using standard methods. Microinjected eggs were then implanted into the oviducts of pseudopregnant ICR females (~20 embryos per recipient). (Methods provided by VCU Transgenic/Knockout Mouse Core).

2.3 Genotyping of Lin52 S28A Knockin Mice

At weaning, DNA was purified from 5-mm tail snips and genotyped by an allele-specific PCR protocol. The protocol involved two separate PCR reactions using a common reverse primer (5'-AGGAGATGAACAAATGCTTTGTGC-3'), paired with either an S28A-specific (5'-TTTGAGAAACTTGACCGTGCAG-3' [mutations underlined]) or a WT-specific (5'-TTTGAGAAACTTGACCGTGCCT-3') forward primer, yielding allele-specific 320-bp products (Figure 8A). *Slc6a2* gene primers (5'-TTAACGTGCTAGGGGTGTAGTGTG-3 and 5'-TTTAGCCTGCTGTTGGGCAGAGTC-3') were included in both reactions, generating a 604-bp internal control product. A second genotyping protocol used primers that flanked exon 2 (5'-TTGAGACCTGACTTTCTTAAACAC-3' and 5'-AGGAGATGAACAAATGCTTTGTGC-3'), and generated 579-bp products for both WT and S28A alleles. Subsequent digestion with AluI cut the WT PCR product into 496-bp and 83-bp fragments and cut the S28A PCR product into 281-bp, 215-bp, and 83-bp fragments (Figure 8B). One potential founder was selected for breeding and further characterization of the line, including DNA sequencing (Fig. 7C). (Methods provided by VCU Transgenic/Knockout Mouse Core).

2.4 Characterization of S28A Lin52 Mice

Homozygous S28A, homozygous wild type, and heterozygous mice were weighed once a week by VCU Mouse Cancer Model Core personnel using a digital scale, and the data were

recorded with Study Director software (StudyLog). Mice were observed at least twice a week for any health issues and were sacrificed when they reached the humane endpoint, as outlined in the IACUC approved protocol. Mice were entered into the study as they were bred, weaned, and genotyped by VCU Transgenic/Knockout Mouse Core. A total of 27 mice were enrolled over the course of the 10-month study. Tissues were collected at time of sacrifice for use in future investigations.

2.5 Cell Culture

Primary mouse embryonic fibroblasts (MEFs) were received from Dr. Jolene Windle at the VCU Transgenic/Knock-out Mouse Core. Cells were taken from wild type and genetically engineered embryos homozygous for the S28A mutation in Lin52. Immortalization was done using the 3T3 serial passaging protocol (Xu, 2005). Phoenix cells were obtained from American Type Culture Collection (ATCC). Cells were cultured in Dulbecco's modified medium (DMEM, Corning Cat# 15-013-CV) supplemented with 1% (v/v) GlutaMax (Life Technologies, Cat# 35050-61), 1% (v/v) Penicillin/Streptomycin (Corning, Cat# 30-002CI) and 10% (v/v) Bovine Calf Serum (GE Healthcare, Cat# SH30072.03). Cells were incubated at 37°C with 5% CO_2 in sterile conditions. When passaged, cells were washed once with 1X PBS (Corning, Cat# MT21-031-CV), detached with Trypsin/EDTA (Gibco, Cat# 25200-056) and resuspended in fresh growth medium. Cells were counted either manually using a hemocytometer (Hausser Scientific) or with the automatic CytoSMART Corning Cell Counter.

2.6 Production of Retroviral Particles

Virus conditioned medium (VCM) was produced by the transfection of Phoenix packaging cells and using pMSCV-CTAP or pWZL retroviral vectors. The GFP, Lin52, and S20C Lin52 retroviral constructs were previously generated by L. Litovchick. For each separate transfection, Phoenix cells were plated in a 10 cm dish with complete medium and allowed to grow to 75% confluency. Plates were transfected with 3 µg pMSCV or pWZL plasmid containing

the gene of interest along with 1.5 µg pCMV-GagPol packaging plasmid and 1.5 µg pCMV-VSVG envelope plasmid. 500 µl of OptiMEM medium (Life Technologies, 31985070) and 18 µl of polyethylenimine were also added to the transfection.

2.7 Generation of Stable Cell Lines

MEFs were plated at 100,000 cells per well in a 6 well plate and allowed to attach overnight. The media was aspirated off and replaced with 1 mL fresh media mixed with 10 µg/mL polybrene and 1 mL of VCM. Cells were infected again the next morning by replacing the media in the same manner. Fresh media was given the next day and cells were allowed to rest overnight. Antibiotic selection was performed with media containing either 1 µg/mL puromycin or 2 µg/mL blasticidin depending on the vector used. Selection continued until the uninfected control cells were dead plus one day. Retroviral vectors used were pWZL_GFP, pWZL_HRAS^{G12V}, pMSCV_GFP, pMSCV_Lin52, and pMSCV_S20C Lin52.

2.8 Preparation of Cell Lysates

Cells were washed twice with PBS and covered with 1 mL of cold PBS containing phosphatase inhibitors (Calbiochem, Cat# 524625) at a 1:500 dilution and a cocktail of protease inhibitors (Calbiochem, Cat#539131) at a 1:100 dilution. The cells were then scraped from the plate and collected by centrifugation. Resulting pellets were either frozen at -80°C or lysed with EBC lysis buffer (Boston BioProducts, Cat# C-1410) containing phosphatase (1:500) and protease inhibitors (1:1000), plus β-ME (BioRad, Cat# 1610710) at a dilution of 1:10,000 for 10 minutes. Following lysis, cell extracts were clarified by centrifugation at 14,000 g for 15 minutes at 4°C. Protein concentration was estimated using BioRad DC Assay and normalized by dilution with EBC.

2.9 Immunoprecipitation

After normalizing the protein concentrations, a 50-100 µl aliquot of each sample was set aside as an input control and 4X LDS sample buffer (Boston BioProducts, Cat# BP-158) with β-

ME was added at a volume that reduced it to 1X. The inputs were incubated for 7 minutes at 95° C. Each remaining sample was mixed with suspension of 20 µl of Protein A Sepharose beads in 80 µl of EBC (GE healthcare, Cat# 17-0780-01), and 1 µg of antibody. Samples were left overnight on a rocker at 4°C. Beads were collected by centrifugation at 10,000 g at 4°C for 30 seconds. Beads were then washed four times with EBC to remove any unbound proteins. The beads were resuspended with 1X sample buffer and incubated at 95°C for 7 minutes. If not used immediately for western blotting, samples were kept at -80°C.

2.10 Western Blotting

Samples were resolved using ready-made minigels gels (BioRad Cat# 4569034) or 4-20% Criterion TGX Precast gel (BioRad Cat# 567-1094), and transferred to nitrocellulose membrane (Amersham, Cat# 10600006) by semi-dry electrophoretic transfer (15V, 40 min). The membrane was blocked for 1 hour in 3% non-fat dry milk in TBST buffer containing 1X Tris buffered saline (TBS) (Boston BioProducts, Cat# BM-300) and 0.05% Tween-20 (BioRad 21 Cat# 1610781). Membranes were incubated with primary antibodies diluted in blocking buffer overnight at 4°C and washed three times with TBST. Blots were then incubated with horseradish peroxidase (HRP)-conjugated secondary antibodies (anti-rabbit or anti-mouse) diluted in 1% milk for one hour at room temperature (RT) followed by chemiluminescence detection. Protein bands were visualized using X-ray films (Fuji Film, Cat# 41101003, 41101004) or digital images taken with the BioRad multi-imager (ChemiDoc MP). If re-probing was needed, membranes were stripped with Restore Western (Thermo Scientific, Cat# 46430).

2.11 Antibodies

Protein	Vendor	Catalog #
B-Myb	EMD Millipore	MABE886
Cyclin A	Santa Cruz	sc-596
Cyclin D1	Santa Cruz	sc-20044
Cyclin D3	Santa Cruz	sc-182
E2F1	Cell Signaling	37425
GFP	Cell Signaling	2956S
HRAS	Santa Cruz	sc-520
LIN37	Bethyl	BL2983
LIN52	Bethyl	BL2991
p130	BD Transduction Labs	610262
pRb	Cell Signaling	9309
Rabbit IgG	Bethyl	P120-101
Vinculin	Sigma	V9131

2.12 Proliferation Assays

MEFs were plated at 100,000 cells/well in 6 well plates with either two or three technical repeats. The cells were then trypsinized and counted the following day, considered to be day 1, as well as on day 3 and day 5 using the CytoSMART Cell Counter. For counting, cells were washed with PBS, incubated with 0.5 mL Trypsin/EDTA, resuspended in complete medium, and spun down. The media was aspirated, and pellets were resuspended in the same volume of fresh medium. An aliquot of this suspension was then mixed with Trypan blue (VWR, Cat# 97063-702) at a 1:1 ratio for detection of dead cells. A total of 8 counts were taken for each sample, 4 different fields from each side of the hemocytometer. These numbers were averaged to supply one count for each sample and technical repeats were then averaged. Each experiment was repeated at least three times, and values were averaged for statistical analysis. Significance was calculated using a two-tailed Student's T-test assuming equal variances.

2.13 Senescence Associated Beta Galactosidase Assays

To trigger a senescence response, MEFs were infected with pWZL_HRAS^{G12V} or pMSCV_GFP retroviruses followed by selection on blasticidin. 5-7 days post infection cells were

washed with PBS, fixed with 2% formaldehyde and 0.2% glutaraldehyde in PBS, and stained with a solution containing 20 mg/mL 5-bromo-4-chloro-3-indolyl-β-D-galactopyranoside (X-gal), molecular biology grade water, 1 M $MgCl_2$, 5 M NaCl, 100 mM potassium ferricyanide, 100 mM potassium ferrocyanide, and 0.2 M citric acid/sodium phosphate buffer (pH 6.0). Cells were incubated overnight at 37° C. The next day cells were washed twice with PBS and imaged with an inverted tissue culture microscope. Quantification was done by manually counting the percentage of SA β-gal positive cells using images taken at 4x magnification.

2.14 EdU Staining

Prior to staining, MEFs were plated at 100,000 cells per well on sterilized coverslips in a 6-well plate, and serum starved for 48 hours with media supplemented with 0.5% calf serum. Cells were released from starvation with addition of 10% calf serum media for the indicated amount of time. EdU staining was performed using iClick™ EdU Andy Fluor 488 Imaging Kit (GeneCopoeia, Cat# A003). Two hours before each timepoint half of the media was replaced with media containing 30 μM EdU, for a final concentration of 15 μM. Cells were fixed on coverslips with 3.7% formaldehyde in PBS for 15 minutes before washing with 3% Bovine Serum Albumin (BSA) in PBS. 1 mL of 0.5% Triton® X-100 in PBS was used for permeabilization. Cells were left to incubate at RT for 20 minutes before washing with BSA. 500 μL of iClick reaction cocktail, which includes the Andy Fluor 488 azide, was added to each well. Plates were then incubated for 30 minutes at RT, protected from light. DNA was counterstained with Hoechst at 1:1000 dilution in PBS. Coverslips were directly mounted onto slides and imaged with an Olympus inverted fluorescent microscope.

2.15 FACS Cell Cycle Analysis

MEFs were grown in p150 plates until approximately 80% confluency and synchronized by serum starvation as described above. After collection in 15 mL Falcon tubes, cells were fixed with dropwise addition of 5 mL cold 70% ethanol while vortexing and stored at 4° C. The day of

the analysis, cells were centrifuged at 4000 rcf for 10 minutes and the ethanol was removed. Cells were resuspended in PBS followed by centrifugation before addition of 1 mL PBS with 100 µg/mL RNase A and 50 µg/mL propidium iodide and incubated for 2 hours at RT in the dark. Samples were filtered using filter top flow cytometry tubes and vortexed briefly before the analysis. Propidium iodide staining of DNA was measured with the BD FACSCanto™ II Analyzer and FACSDiva software at the VCU Flow Cytometry Shared Resource Core.

CHAPTER THREE: RESULTS

3.1 Generation of the S28A Lin52 Mouse Model

Previously, it has been shown that mutation of the serine 28 site of Lin52 from serine to alanine (S28A) prevents both DYRK1A phosphorylation and DREAM assembly in mammalian cells (Litovchick et al., 2011). Therefore, we decided to generate an *in vivo* mouse model of DREAM disruption in collaboration with the VCU Transgenic/Knockout Mouse Core. The CRISPR/Cas9 editing system was employed to introduce the S28A mutation into the Lin52 gene of C57BL/6J mice. Figure 7 shows the location and sequence of the wild-type and modified Lin52 alleles. Three base substitutions resulted in the serine to alanine mutation of codon 28, added an AluI restriction site, and removed the PAM Cas9 recognition sequence (Figure 7B).

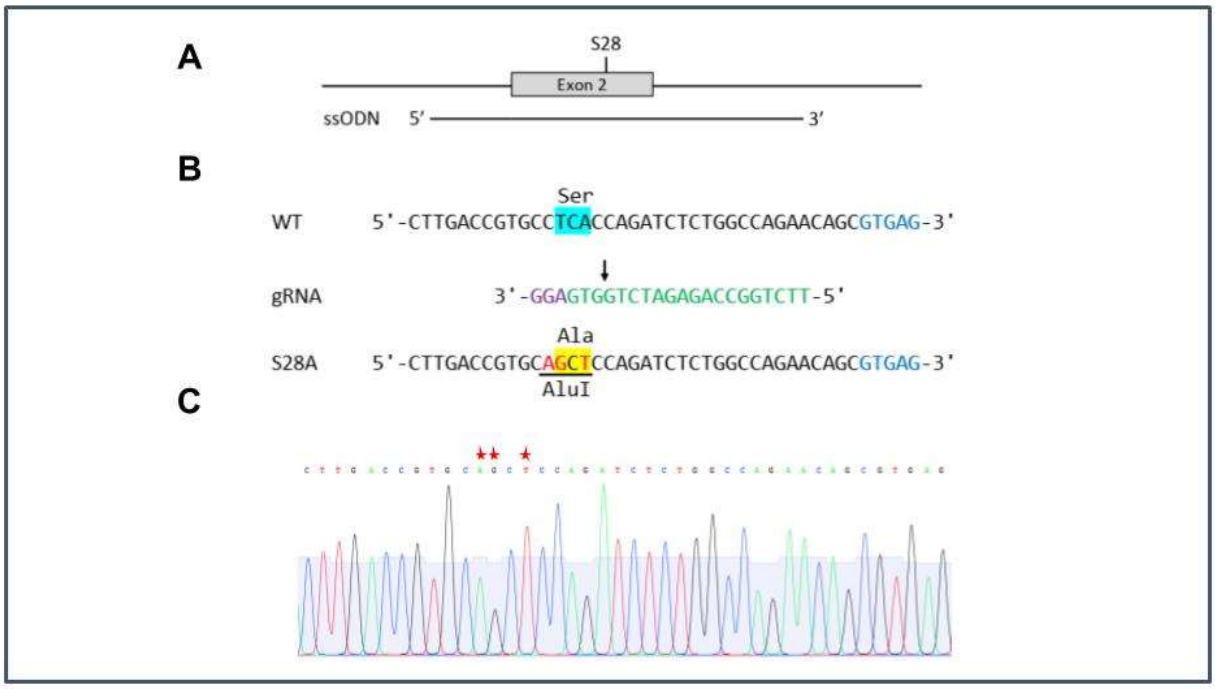

Figure 7. Generation of S28A Lin52 knockin mice using CRISPR/Cas9. A) Diagram of Lin52 exon 2, indicating the locations of the S28 codon and 200-base sense-strand ssODN repair template. B) Sequences of the wild-type (WT) Lin52 allele, the gRNA protospacer (green) and PAM (purple), and the S28A allele (with base substitutions in red). The Cas9 cleavage site (arrow), codon S28 (highlighted in turquoise), codon S28A (highlighted in yellow), start of intron 2 (blue), and AluI site in the S28A sequence (underlined) are indicated. C) Partial sequencing chromatograph from a homozygous S28A knockin mouse corresponding to the region of the S28A allele in B. Stars indicate the locations of the base substitutions in the chromatograph. (Figure and legend provided by the VCU Transgenic/Knockout Mouse Core).

A heterozygous crossing of these genetically engineered mice produced 6 pups, who were genotyped using samples of tail snippings. Two different PCR protocols were used, one making use of allele specific primers and the other the AluI restriction site. Samples were run with S28A and wild-type Lin52 allele specific forward primers to produce PCR products corresponding to genotype (Figure 8A). In the second protocol, exon 2 flanking primers were used to generate 579 bp products from both alleles prior to digestion with the AluI enzyme. Wild type alleles are cut into two fragments and S28A alleles are cut into three, allowing for genotype discrimination (Figure 8B). Of the two homozygous pups, one was chosen as a potential founder and genotype was confirmed by DNA sequencing (Figure 7C).

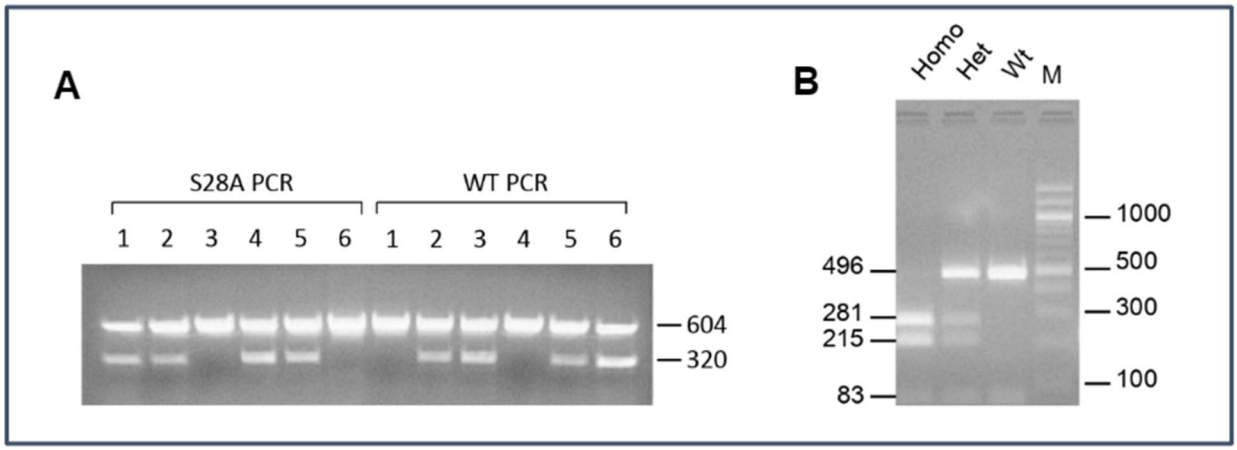

Figure 8. Genotyping of S28A Lin52 knockin mice. A) Six pups from a S28A Lin52 heterozygote x heterozygote mating were genotyped by an allele-specific PCR protocol. The protocol involved two separate PCR reactions using a common reverse primer paired with either a S28A-specific or a WT-specific forward primer, yielding allele-specific 320-bp products. An internal control primer pair generating a 604-bp product was included in all reactions. Mice #1 and #4 from this litter are homozygous S28A knock-ins, #2 and #5 are heterozygotes, and #3 and #6 are WT. A 703-bp region containing exon 2 from mouse 4 was sequenced to generate the chromatograph shown in Figure 7C. The six pups from A were also genotyped by a second PCR protocol using primers flanking exon 2, followed by AluI digestion of the 579-bp products. AluI cuts the WT product into 496-bp and 83-bp fragments, and cuts the S28A product into 281-bp, 215-bp, and 83-bp fragments. (Figure and legend provided by VCU Transgenic/Knockout Mouse core).

The S28A mutation provides an opportunity to study DREAM-specific loss without interfering with other protein functions. Importantly, the functions of the MuvB core, pocket proteins, DYRK1A, and other cell cycle regulatory proteins remain intact. Unlike the previous mouse models disrupting various components of the DREAM complex, our homozygous S28A mice are viable and do not appear to be developmentally abnormal at birth. Therefore, this model is suitable for investigating the physiological role of DREAM both during development and in the adult organism.

3.2 DREAM Inhibition Increases Proliferation

After establishing the S28A mouse model, fibroblasts were extracted from wild type and S28A homozygous embryos for use in cellular studies. These mouse embryonic fibroblasts (MEFs) were immortalized by the NIH 3T3 serial passaging protocol to establish the wild-type

Lin52 and S28A Lin52 MEF cell lines. Lack of DREAM assembly was confirmed with immunoprecipitation of MuvB component LIN37 and probing for p130 and B-Myb. As shown in Figure 9A, p130 is pulled down with LIN37 in wild type cells, but not in the mutant cell line. In addition, B-Myb is co-precipitated with LIN37 in S28A Lin52 cells as is expected due to increased B-Myb expression and availability of the MuvB core.

Previous studies have shown that DYRK1A overexpression enhances DREAM and suppresses cell growth, while inhibition of DYRK1A does the opposite and promotes proliferation (Litovchick et al., 2011). Additionally, ectopic expression of S28A Lin52 rescued the DYRK1A-mediated growth suppression in cells. These observations, together with the known cell cycle promoting functions of genes repressed by DREAM, led us to hypothesize that S28A Lin52 MEFs would proliferate faster than wild-type Lin52 MEFs. To test this hypothesis, we performed a proliferation assay and found that S28A MEFs indeed grow at a rate significantly faster than wild-type MEFs (Figure 9B). This finding supports the role of DREAM in regulating cell proliferation.

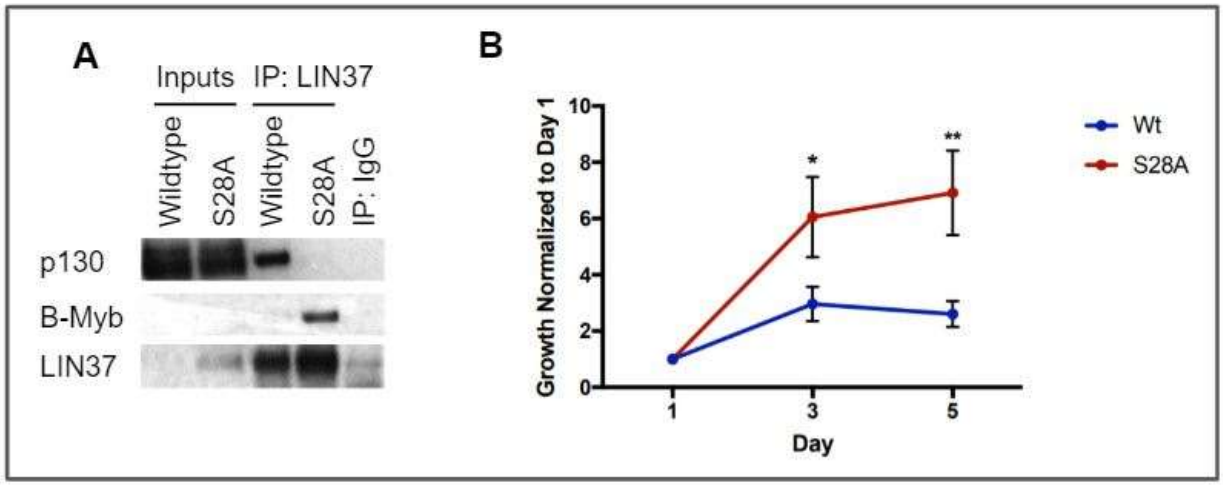

Figure 9. S28A Lin52 mutation prevents DREAM assembly and increases cell proliferation. A) Loss of DREAM assembly was confirmed by immunoprecipitation of MuvB subunit LIN37 and immunoblotting with antibodies against p130, B-Myb, and LIN37 using lysates from wild-type Lin52 and S28A Lin52 MEFs. B) S28A Lin52 MEFs have an increased proliferation rate compared to wild-type (Wt) MEFs. Results are average of three biological replicates. (* denotes $p<0.05$, ** denotes $p<0.001$)

3.3 S28A Lin52 MEFs Display Deregulation of the Cell Cycle

The increased proliferation of S28A Lin52 MEFs suggests they are spending less time in G0/G1 and progressing faster through the cell cycle. To investigate cell cycle progression without DREAM present, we synchronized the wild-type and S28A Lin52 MEF cell lines and measured the expression of cell cycle markers over time following stimulation to re-enter the cell cycle. After 48 hours of serum starvation wild-type MEFs have little to no expression of B-Myb, cyclin A, or E2F1, whereas S28A Lin52 MEFs demonstrated increased expression of these proteins (Figure 10). These proteins are encoded by DREAM target genes with peak expression at the G1/S transition or in S phase. Therefore, their presence under the conditions of G0/G1 arrest could confirm lack of DREAM target repression and failure to fully arrest in S28A Lin52 cells. Levels of the E2F1 transcriptional activator are highest at the end of G1, and cyclin A facilitates both G1/S and S/G2 transitions. Levels of these three markers are higher in S28A Lin52 MEFs at all three release timepoints, suggesting these cells are ahead of the wild type in the cell cycle. As an example, based on the expression profiles of these proteins, S28A Lin52 MEFs are more likely to be in G1/S, S phase, or G2 than wild-type MEFs at 17 hours post release.

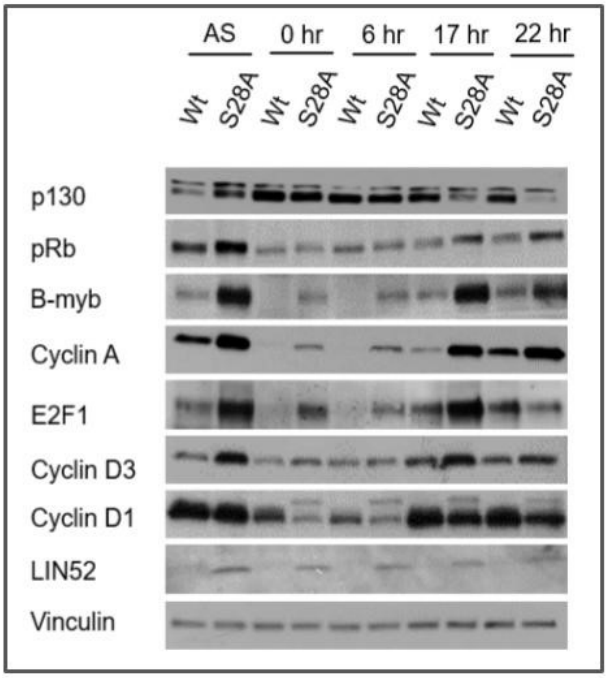

Figure 10. Cell Cycle Marker Expression in Synchronized Wt and S28A Lin52 MEFs. MEFs were serum starved for 48 hours and released for the indicated timepoints before collection and Western blotting for cell cycle proteins. (AS = asynchronous, hr = hour/hours)

Cyclin D1 and D3 are not DREAM targets and are the first cyclins activated when a cell starts a new cycle. Both cyclins interact with CDKs to inactivate Rb and are required for G1/S transition. Levels of cyclin D3 are increased in asynchronous S28A Lin52 cells, as well as at 0, 17, and 22 hours post release. Cyclins D1 and D3 have been seen to have differing levels of response to growth factors, with levels of cyclin D1 being more highly induced (Paternot et al., 2006). This could explain the difference in expression between the cyclins seen here. The double bands observed in the S28A lanes of cyclin D1 could correspond to an increase in phosphorylation, possibly at the Thr286 site, which controls cyclin D1 export from the nucleus and proteolytic degradation in S phase (Alt et al., 2000). While Rb expression does not change dramatically throughout the cell cycle (Figure 2B), it is elevated in S, G2, and M phases, as is seen in asynchronous, 17, and 22-hour S28A Lin52 cells. p130, on the other hand, is decreased in these cells compared to the wild-type MEFs at 17 and 22 hours, possibly due to an increased

proteosomal degradation that was previously observed for p130 during S-phase. Interestingly, the protein levels of S28A Lin52 were increased compared to the wild-type Lin52, consistent with our previous observation that this mutation increases Lin52 protein stability (Iness et al., 2019).

To investigate cell cycle progression in a more quantifiable manner, we performed a cell cycle analysis using propidium iodide (PI) staining of DNA and fluorescence activated cell sorting (FACS). Wild type and S28A Lin52 MEFs were again serum starved and released before fixation and staining. The two cell lines displayed differing cell cycle profiles whereby the S28A Lin52 MEFs have less cells with a 2n DNA complement at 0 hours than wild-type MEFs, suggesting a possible decreased ability to arrest. Importantly, there is an increase in the number of cells having a DNA content between 2n and 4n when comparing S28A Lin52 to wild-type cells at 22 hours (Figure 11) indicating that there are more S28A Lin52 MEFs with active DNA synthesis at this time than the wild type. This is further evidence of more rapid cell cycle progression in our model of DREAM inhibition.

As a complement to our FACS data, we also performed a proliferation assay using the thymidine analog 5-Ethynyl-2´-deoxyuridine (EdU). This compound is incorporated into DNA during replication, allowing for tracking of DNA synthesis. Our results agree with those from the cell cycle marker and flow cytometry analysis. As is seen in Figure 12, the S28A Lin52 cell line appears to have a higher ratio of EdU positive cells than the wild type, indicating more DNA synthesis activity at almost all timepoints. In addition to the earlier experiments, this observation supports the conclusion that loss of DREAM leads to deregulation of the cell cycle.

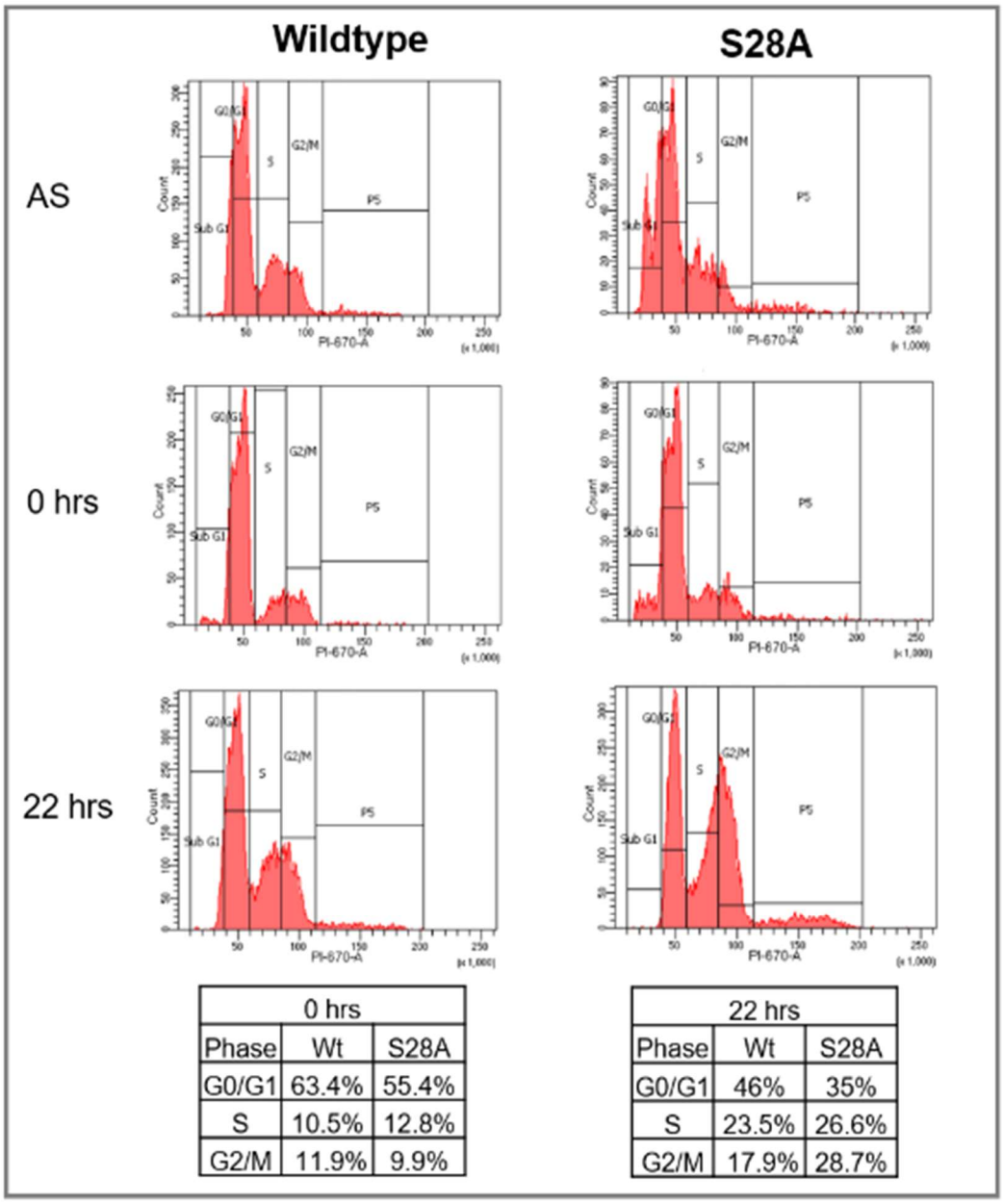

0 hrs		
Phase	Wt	S28A
G0/G1	63.4%	55.4%
S	10.5%	12.8%
G2/M	11.9%	9.9%

22 hrs		
Phase	Wt	S28A
G0/G1	46%	35%
S	23.5%	26.6%
G2/M	17.9%	28.7%

Figure 11. FACS cell cycle analysis of Wt and S28A Lin52 MEFs. Histograms depicting cell counts by DNA content and tables of cell percentage per phase at 0 and 22 hours.

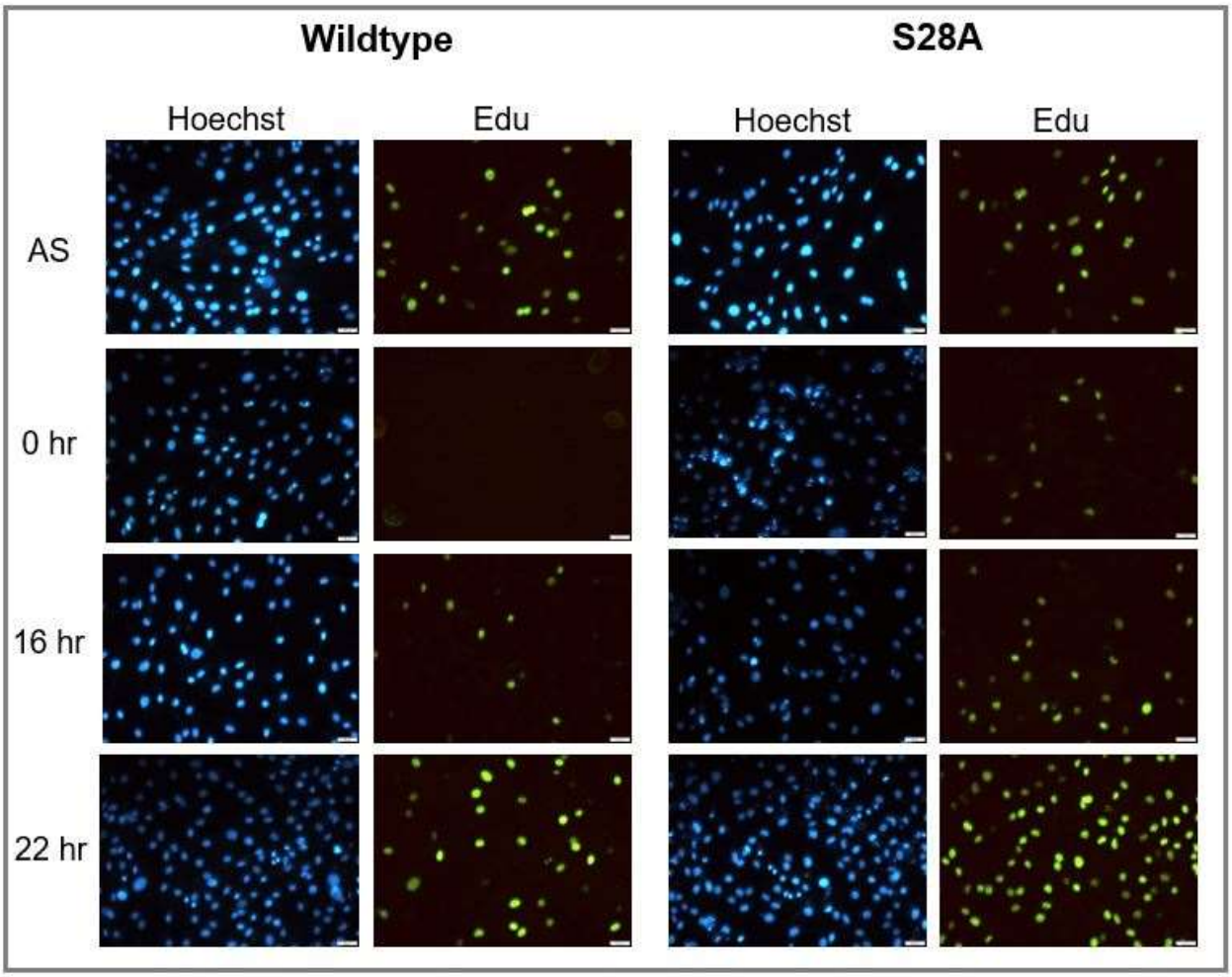

Figure 12. S28A MEFs display increased DNA synthesis. Fluorescent microscopy images of EdU and Hoechst nuclear counterstained MEFs taken at 10x magnification.

3.4 DREAM is Required for Oncogenic Ras Induced Senescence

Expression of the oncogenic Ras allele, $HRAS^{G12V}$, leads to senescence, or permanent cell cycle arrest, through pathways that trigger repression of cell cycle regulated genes (Serrano et al., 1997). This led to investigating whether DREAM was necessary for the downregulation of these genes and entry into senescence. Disruption of DREAM by DYRK1A knockdown or ectopic expression of S28A Lin52 was shown to reduce levels of senescence associated beta-galactosidase (SA β-gal) in human fibroblasts expressing $HRAS^{G12V}$ (Litovchick et al., 2011). To examine this effect in cells without the presence of any intact LIN52, we performed the same assay with the wild-type and S28A Lin52 MEF cell lines. The $HRAS^{G12V}$ allele was delivered

through a viral vector and the SA β-gal assay was performed several days post selection. SA β-gal was visibly much more active in wild type than S28A Lin52 cells, implying that DREAM is required for senescence in response to oncogenic HRAS^{G12V} (Figure 13A). The difference in HRAS^{G12V} expression between the two cell lines should be noted (Figure 13B) and possible explanations are given in Chapter Four.

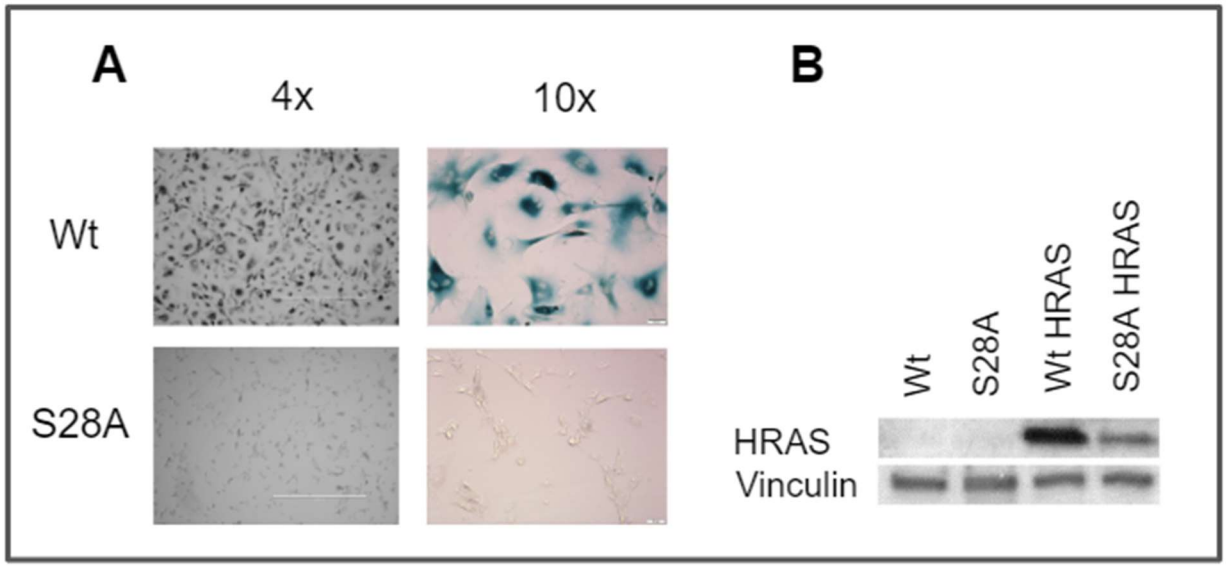

Figure 13. S28A Lin52 MEFs fail to senesce. A) SA β-gal assay using wild type and S28A Lin52 MEFs expressing HRAS^{G12V}. B) Western blot confirming HRAS expression in the indicated cell lines. Vinculin serves as loading control.

3.5 Restoration of DREAM Slows Proliferation

Because ectopic expression of S28A Lin52 has been shown to interrupt DREAM in cells with a normal Lin52 genotype, we hypothesized that expression of wild-type Lin52 will rescue DREAM assembly in S28A Lin52 MEFs. If true, we further hypothesized that rescuing DREAM would slow proliferation of these cells. S28A Lin52 MEFs were infected with wild-type Lin52, a vector control containing GFP, and another mutant form of Lin52. This allele has a mutation causing the serine 20 residue to be replaced with cysteine (S20C) in the LXSXE motif, mimicking the LXCXE motif of viral oncoproteins that allows them to competitively bind p130. This mutation has been previously shown to increase affinity of the p130-Lin52 interaction,

therefore we expected S20C Lin52 expression to result in a stronger DREAM rescue than wild-type Lin52. Rescue of the complex was confirmed with LIN37 pull down and probing for p130 and B-Myb. As is seen in Figure 14A, expression of wild-type Lin52 and S20C Lin52 both rescue binding of p130 to the MuvB core, more so in S20C cells as we hypothesized. Probing for LIN52 confirmed the expression of ectopic Lin52 in the wild type and S20C Lin52 infected cell lines, which present as the higher migrating bands due to a presence of a dual HA-Flag epitope tag (Figure 14B). The decrease in endogenous LIN52 with its ectopic expression has been observed before in our laboratory (Litovchick et al., 2011, Iness et al, 2019). To test our hypothesis that restoration of DREAM slows cell growth, we performed the same proliferation assay that was shown in Figure 9B where equal number of cells were plated for each cell line, and counted at days 1, 3 , and 5. We found the two rescue lines did, in fact, proliferate significantly slower than the S28A Lin52 parental line (Figure 14C). No difference in proliferation was observed between the expression of wild-type Lin52 and S20C Lin52. This finding further confirms the relationship between cell division and status of the DREAM complex.

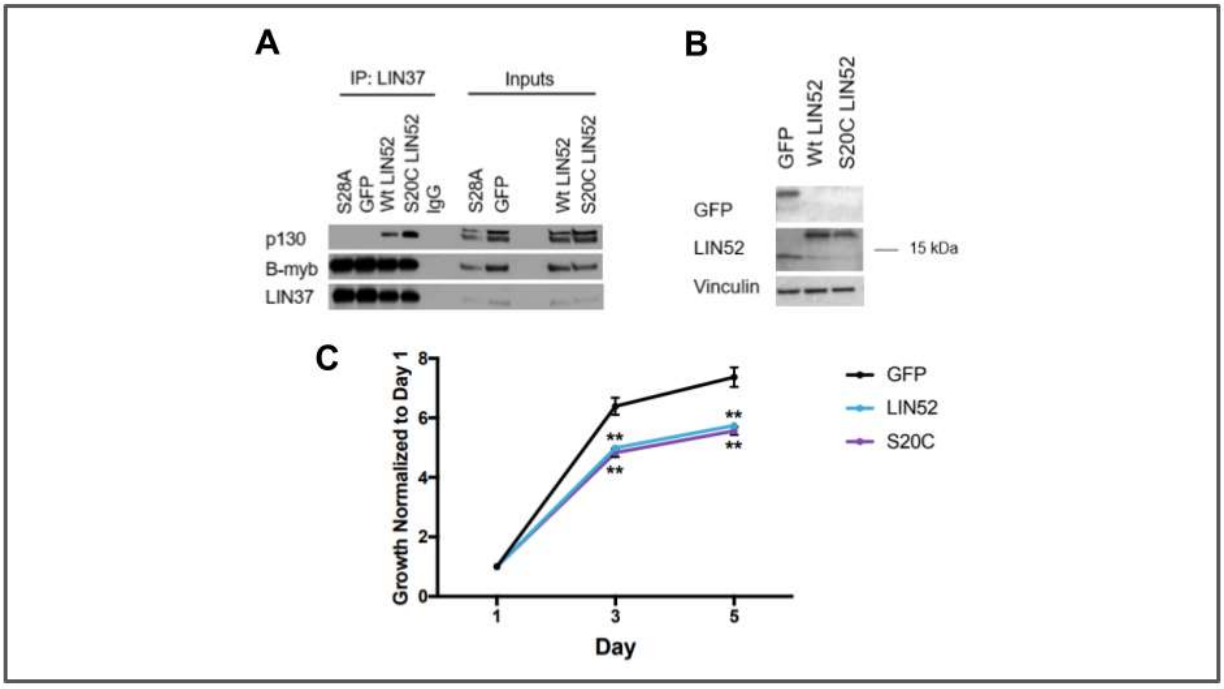

Figure 14. Expressing wild-type or S20C Lin52 in S28A Lin52 MEFs rescues DREAM assembly and slows cell growth. A) Immunoprecipitation of MuvB component LIN37 and immunoblot with antibodies against p130, B-Myb, and LIN37 with lysates from S28A Lin52 MEFs expressing GFP, Wt Lin52, or S20C Lin52. Presence of p130 or B-Myb binding indicates formation of the DREAM or MMB complexes, respectively. B) Western blot confirming expression of ectopic Wt and S20C Lin52 and GFP in S28A Lin52 DREAM rescue and control cells. C) Restoring DREAM decreases proliferation rate in S28A Lin52 MEFs. Result is the average of three biological replicates. (** denotes $p<0.001$)

3.6 Rescue of Senescence with DREAM

Seeing as the SA β-gal activity of $HRAS^{G12V}$ expressing S28A MEFs was drastically reduced in comparison to $HRAS^{G12V}$ expressing wild-type MEFs, and that introduction of wild-type Lin52 rescues DREAM, we hypothesized that re-expressing the wild type and S20C Lin52 would also return senescence ability to S28A Lin52 MEFs. To test this, we used the same methods as above: infection with $HRAS^{G12V}$ expressing retrovirus followed by SA β-gal assay. We observed an increase in SA β-gal activity in the wild type and S20C Lin52 expressing lines compared to the two control lines (Figure 15A and B), with S20C displaying the most activity. This result indicates that rescue of DREAM may increase oncogenic Ras induced senescence in DREAM-less cells and further confirms a role for DREAM in entering a senescent state.

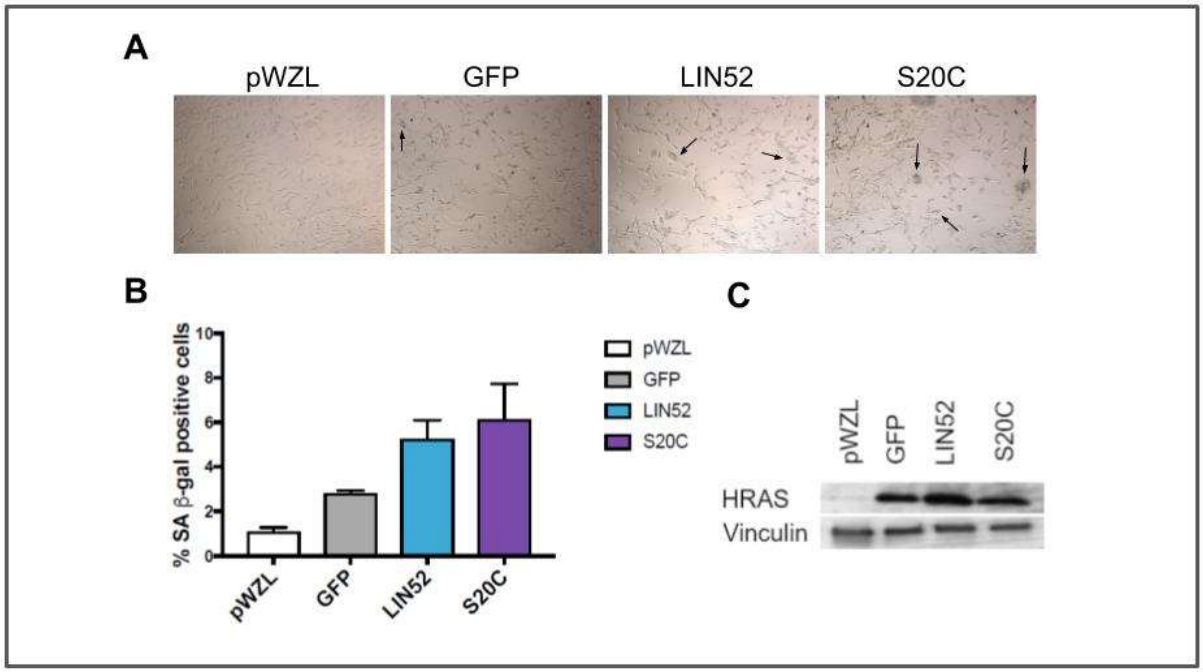

Figure 15. Restoring DREAM increases oncogenic Ras induced senescence. A) Images of DREAM rescue cell lines, pWZL vector control and GFP control cell lines after SA β-gal assay, taken at 4X magnification. Arrows point to SA β-gal positive cells. B) Quantification of assay showing increased β-gal activity in the wild-type Lin52 and S20C Lin52 cell lines. 3 fields containing 200-300 cells were counted and averaged for each cell line. C) Western blot confirming the expression of HRAS. Vinculin serves as loading control.

3.7 Characterization of S28A Lin52 Mice

Previous mouse models of DREAM loss have not been viable due to disruption of pocket protein function or the MMB complex (see section 1.12), preventing characterization of these mice past a few days post birth. Therefore, to investigate possible short- or long-term physiological effects of DREAM inhibition, we generated a S28A Lin52 knock-in mouse model in collaboration with the VCU Transgenic/Knockout Mouse Core. For the initial phenotype characterization study of our model, the genotyped mice were observed several times a week for any overt health issues and body weight was recorded once a week. This is an ongoing, initial health screen of the mutant DREAM-less mice and as such we did not have clear expectations at the beginning. However, considering the function of DREAM, one point of interest was potential development of tumors and their location.

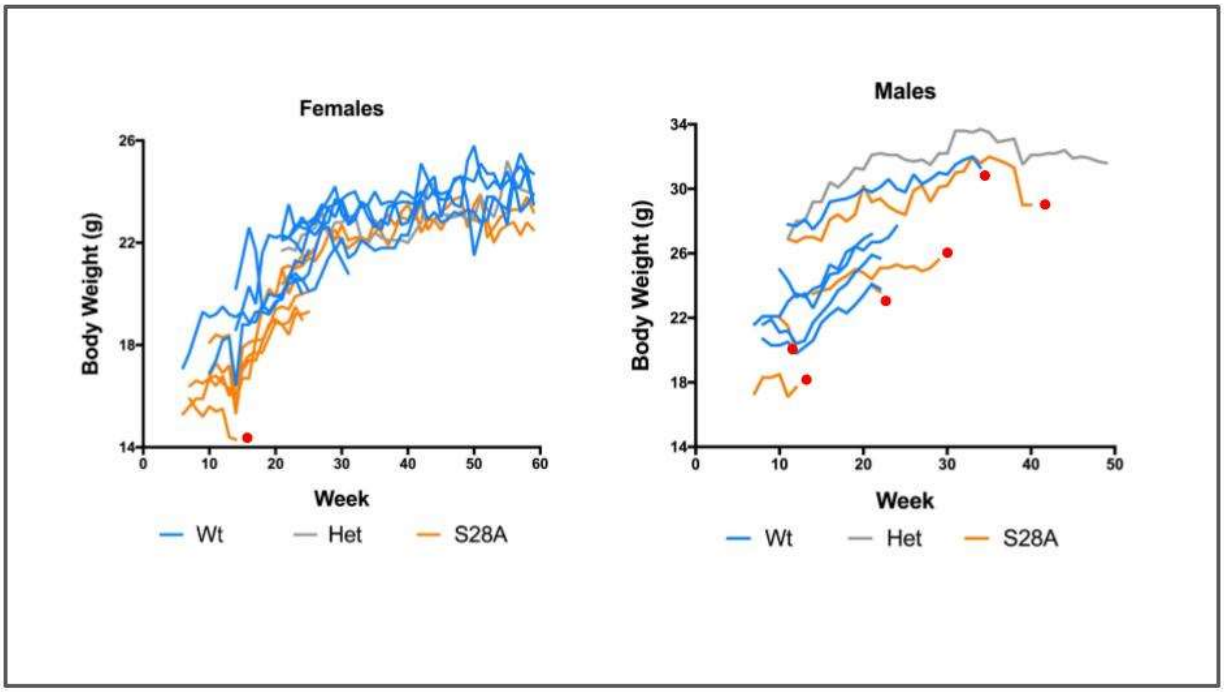

Figure 16. S28A Lin52 mice tend to weigh less than age matched Wt mice. Body weight by age of 11 male (5 S28A, 1 heterozygous, and 5 Wt) and 16 female mice (7 S28A, 1 heterozygous, and 8 Wt). Red dots indicate mice that reached the humane endpoint and were sacrificed.

Although the homozygous S28A Lin52 mice do not appear visibly smaller, they tend to weigh less than their wild type counterparts (Figure 16). More time and a higher sample size will further elucidate this phenotype and its significance. In this study, there was a sex dependent shortening of lifespan seen in S28A Lin52 mice. All 5 of the S28A Lin52 homozygous male mice required sacrificing due to signs of distress at some point in this study. These mice became weak, displayed a hunched posture, began losing weight, and two of them had skin lesions on the scruff of the neck. The ages of sacrifice of these mice range from 12 weeks to 40 weeks, with an average of 23.2 weeks and a median of 22 weeks of age. The average lifespan of wild-type C57BL/6J male mice is 878 ± 10 days (125 weeks) (Kunstyr and Leuenberger, 1975), suggesting that S28A Lin52 mice have reduced fitness or longevity. In contrast, the only other two mice in our study that had to be sacrificed due to failure to thrive were a 34-week-old wild-type male and a 13-week-old S28A Lin52 female. This indicates a potential health disparity in

S28A Lin52 males, however more studies are needed to clearly define the underlying mechanisms. The only two heterozygotes in our study (one female, one male) have not had any issues so far and, in the case of the male, have a slightly higher body weight than wild type. No tumors or abnormal tissues were observed during necropsy, however the age of even the oldest mouse was only about a quarter of the average lifespan. Finally, we did not observe any overt behavioral differences between these groups of mice. As the study continues, we will develop a more complete characterization of the impact of the DREAM loss *in vivo*.

CHAPTER FOUR: DISCUSSION

4.1 DREAM Loss Deregulates the Cell Cycle and Promotes Proliferation

The DREAM complex forms during G0/G1 to bind and repress cell cycle genes, aiding arrest of the cycle. DREAM formation depends on the phosphorylation of LIN52 at S28 by DYRK1A, which allows the pocket protein p130 to bind the MuvB core. We have shown that the S28A Lin52 mutation disrupts DREAM formation and increases levels of the positive transcriptional regulator complex MMB. This disruption leads to the upregulation of cell cycle regulatory proteins (E2F1, B-Myb, cyclin A and others), accelerated progression from G0/G1 to S phase, and increased proliferation in MEFs. This study focused mainly on the G0/G1/S phase transition, but a loss of DREAM would also be expected to deregulate the MMB targets that are expressed during late S or G2/M phases. Therefore, it would be worthwhile in the future to examine progression through a full cell division cycle and to look for evidence of mitotic defects, such as chromosomal abnormalities. Also, considering these ideas, it would be interesting to investigate whether loss of DREAM can lead to spontaneous cellular transformation because of accumulating genomic instability, potentially facilitated by loss of p53 function. Aberrant expression and activity of the upstream DREAM regulators that are also DREAM/MMB target genes, such as *CCNE*, *CDK2*, and *MYBL2*, are seen in many cancer types (see section 1.10). This suggests that cancer cells that acquired an activating mutation in one of the genes that promote DREAM disassembly could have then established a positive feedback loop to further attenuate the DREAM function. We have shown here that restoration of DREAM in S28A Lin52

MEFs slows proliferation, indicating the overexpression of cell cycle genes was attenuated. This marks the DREAM/MMB complexes as possible targets for slowing the growth of cancerous cells.

4.2 DREAM and Cell Cycle Arrest

We have found that S28A Lin52 MEFs do not arrest the cell cycle with the same efficiency as wild-type MEFs in response to either serum starvation or oncogenic Ras. These cells displayed more DNA synthesis activity after starvation in both the FACS analysis and EdU assay and did not senesce to the level of the wild type in the SA β-gal assay in response to the oncogenic Ras. Cellular arrest regulation is important for maintaining genomic integrity. When DNA damage occurs, the cell cycle is arrested to give the cell the time to repair the damage before dividing. Cells with severe DNA damage are triggered to senesce or die by apoptosis as a protective mechanism to prevent emergence of cancerous clones. If unable to halt the cell cycle, cells may fail to repair DNA damage and divide into daughter cells still containing the genomic alterations. Cells may survive that were not meant to, and continue producing more cells that have a defective cell cycle brake mechanism. Because DREAM has been shown to be a valuable player in both quiescence and senescence, it would be interesting to examine whether DREAM inhibited cells continue to grow after DNA damage. It is important to mention that p53 is an upstream regulator of DREAM assembly. Once activated, p53 induces transcription of the CDK inhibitor p21, which works to stop phosphorylation of p130 and other pocket proteins, resulting in repression of the E2F target genes and cell cycle arrest. Therefore, frequent mutations in the *TP53* gene in cancers add to the importance of characterizing loss of DREAM regulation in cancer pathogenesis.

Other senescence related processes that DREAM could be implicated in are replicative senescence and chemotherapeutic drug efficacy. In theory, deregulation of DREAM could lead to premature senescence or failure to enter replicative senescence when prompted. Many

chemotherapies, such as the CDK4 inhibitor palbociclib, aim to trigger a senescence response in cancer cells, and tumors that lack the ability to arrest the cell cycle are resistant to these kinds of treatments. Targeting the DREAM complex as a method of inducing senescence could potentially aid in the effectiveness of these drugs. Interestingly, when subjected to the quiescence-inducing conditions of serum starvation, we observed a decrease in viability of S28A Lin52 MEFs (data not shown). These cells did not appear to tolerate the lack of mitogenic signals as well as the wild type. We speculate that these cells experience a heightened level of stress when proliferation genes continue to be expressed that conflict with the loss of mitogenic signals, eventually leading to apoptosis. This phenotype still needs to be confirmed and investigated, but it could imply a cell specific, differential response to DREAM inhibition.

Another research focus in addition to the *in vivo* studies of the DREAM-less mouse could be the mechanism of different expression levels between wild type and S28A Lin52 MEFs (Figure 10). This increase of LIN52 in DREAM-inhibited cells has been seen before in our laboratory when using DYRK1A knockdown or DYRK1A kinase inactive cells, as well as the B-Myb-overexpressing human cell lines. This phenotype needs to be further investigated, considering the possibilities that LIN52 is more stable when it is not phosphorylated at the S28 site, or when it is bound to B-Myb instead of p130.

4.3 S28A Lin52 Mice as an *In Vivo* Model of DREAM Disruption

We have demonstrated the S28A Lin52 mouse to be the first viable *in vivo* model for study of the physiological role of DREAM in a mammalian organism. So far, our phenotypic characterization study has found that S28A Lin52 homozygous mice tend to have a decreased body weight, but not to have any obvious health defects. S28A Lin52 males had a shortened lifespan compared to the matched wild-type mice due to failure to thrive, but further studies will be needed to find out the underlying cause for this phenotype. This is a study in progress that will be used to further understand the consequences of DREAM loss in mice. Having

established this model, it can be used for many different studies of the role of DREAM *in vivo*. The health of individual DREAM deficient tissues can be examined by histological means, for example, Ki67 staining for hyperproliferation or SA β-Gal staining for senescence. This model could be crossed with mouse strains containing Kras or Hras mutations, to examine the impact of DREAM loss on tumorigenesis. These mice could be used for testing of novel anti-cancer treatments in a DREAM-deficient environment. Also of note, *DYRK1A* is located within the Down syndrome critical region of chromosome 21 (Shindoh et al., 1996). Our S28A Lin52 model could be used to investigate the role of DREAM in phenotypes of trisomy 21 through crosses with mice models of Down syndrome.

4.4 Experimental Considerations

In the spirit of rigor and transparency, there are several limitations in the above study that should be mentioned. First, we cannot rule out that the cells used for all *in vitro* experiments have developed additional genomic alterations as a result of their immortalization by serial passaging. This process selects for cells that can overcome division limitations, such as replicative senescence, likely as a result of mutations that will then be propagated in daughter cells. The wild type and S28A Lin52 MEF cell lines could have potentially accumulated different alterations, making them less comparable. When performing stress induced senescence experiments it is helpful to know the status of the p53 protein, a main dispatcher of cellular arrest signals in response to genotoxic stress, to avoid misinterpretation of the data. The p53 status of our wild type and S28A Lin52 MEF lines could not be confirmed in time for this study completion. This could be done by inducing p53 expression through methods such as doxorubicin treatment or irradiation, followed by measurement of expression and S15 phosphorylation by Western blotting. Pertinent genes, such as *TP53*, could be also sequenced to find mutations, but a separate study could be required to reveal a full spectrum of genetic alterations using whole genome sequencing and functional assays. Fortunately, our use of the

S28A Lin52 DREAM rescue lines made from the same parental line, which was used as a control, confirmed that the phenotypes demonstrated here were at least in part due to the DREAM disruption. However, we observed less dramatic difference in SA β-gal activity between the rescue and control lines compared to that seen in the wild type and S28A Lin52 cell lines. Therefore, future studies can be performed using additional independently generated primary and immortalized MEF cell lines, as well as our three rescue cell lines (GFP, wild-type Lin52, and S20C Lin52 expressing DREAM-less MEFs), for a more fair and objective comparison.

As seen in Figure 13B, there is an unequal level of HRAS expression in the wild type and S28A Lin52 cell lines. A possible explanation for this could be that S28A Lin52 cells had a decreased efficiency in viral infection compared to control cells. However, the fraction of the surviving cells during selection was very similar to the wild type suggesting that the infection was successful. Another possibility is that S28A Lin52 cells expressing the highest levels of HRAS died, such as they did when subject to serum starvation. To confirm that differences in HRAS expression are specific to S28A Lin52 cell line phenotype, we could measure the expression of HRAS in the unselected wild type and S28A Lin52 MEFs cells immediately after infection, or use a control protein such as GFP, to confirm an equal infection efficiency and post-selection protein levels.

CONCLUSION

In summary, we have found roles for the DREAM complex in regulation of the cell cycle progression and both temporary and permanent cell cycle arrest. We have shown that the S28A mutation of Lin52 interrupts DREAM assembly and increases proliferation of mouse embryonic fibroblasts. These S28A Lin52 MEFs express cell cycle markers under arrest-inducing conditions and continue to overexpress these proteins upon re-entry and progression of the cell cycle. We demonstrate that DREAM-less cells display increased DNA synthesis activity under these conditions as well. These cells also show a dramatic decrease in senescence compared to wild-type cells when exposed to the oncogenic $HRAS^{G12V}$ allele. Through ectopic expression of wild-type or S20C Lin52, we were able to restore DREAM formation in S28A Lin52 MEFs. This restoration slowed proliferation and partially rescued the senescence ability of these cells. We have established our S28A Lin52 mouse strain as an *in vivo* model of DREAM disruption and have begun characterizing these mice. Current evidence suggests S28A Lin52 mice have a subtle phenotype resulting in shortened lifespan in males, which needs to be further investigated. Overall, our study provides insight into the cell cycle deregulation caused by DREAM disruption and gives a first look at this process in a living mammalian organism. Our initial findings suggest DREAM loss could potentially increase tumorigenesis, but further study is necessary to determine valid therapeutic targets that can restore DREAM assembly in tumor cells.

LIST OF REFERENCES

1. Alt, J.R., Cleveland, J.L., Hannink, M., and Diehl, J.A. (2000). Phosphorylation-dependent regulation of cyclin D1 nuclear export and cyclin D1-dependent cellular transformation. Genes Dev *14*, 3102–3114.

2. Attwooll, C., Lazzerini Denchi, E., and Helin, K. (2004). The E2F family: specific functions and overlapping interests. EMBO J *23*, 4709–4716.

3. Beall, E.L., Manak, J.R., Zhou, S., Bell, M., Lipsick, J.S., and Botchan, M.R. (2002). Role for a Drosophila Myb-containing protein complex in site-specific DNA replication. Nature *420*, 833–837.

4. Becker, W., Weber, Y., Wetzel, K., Eirmbter, K., Tejedor, F.J., and Joost, H.-G. (1998). Sequence Characteristics, Subcellular Localization, and Substrate Specificity of DYRK-related Kinases, a Novel Family of Dual Specificity Protein Kinases. Journal of Biological Chemistry *273*, 25893–25902.

5. Ceol, C.J., and Horvitz, H.R. (2004). A New Class of C. elegans synMuv Genes Implicates a Tip60/NuA4-like HAT Complex as a Negative Regulator of Ras Signaling. Developmental Cell *6*, 563–576.

6. Clarke, A.R., Maandag, E.R., van Roon, M., van der Lugt, N.M.T., van der Valk, M., Hooper, M.L., Berns, A., and te Rielef, H. (1992). Requirement for a functional Rb-1 gene in murine development. Nature *359*, 328–330.

7. Classon, M., and Dyson, N. (2001). p107 and p130: Versatile Proteins with Interesting Pockets. Experimental Cell Research *264*, 135–147.

8. Cobrinik, D., Lee, M.H., Hannon, G., Mulligan, G., Bronson, R.T., Dyson, N., Harlow, E., Beach, D., Weinberg, R.A., and Jacks, T. (1996). Shared role of the pRB-related p130 and p107 proteins in limb development. Genes & Development *10*, 1633–1644.

9. DeCaprio, J.A. (2009). How the Rb tumor suppressor structure and function was revealed by the study of Adenovirus and SV40. Virology *384*, 274–284.

10. DeCaprio, J.A., Ludlow, J.W., Figge, J., Shew, J.-Y., Huang, C.-M., Lee, W.-H., Marsilio, E., Paucha, E., and Livingston, D.M. (1988). SV40 large tumor antigen forms a specific complex with the product of the retinoblastoma susceptibility gene. Cell *54*, 275–283.

11. DeGregori, J. (2002). The genetics of the E2F family of transcription factors: shared functions and unique roles. Biochimica et Biophysica Acta (BBA) - Reviews on Cancer *1602*, 131–150.

12. Dick, F.A. (2007). Structure-function analysis of the retinoblastoma tumor suppressor protein - is the whole a sum of its parts? Cell Div *2*, 26–26.

13. Doench, J.G., Hartenian, E., Graham, D.B., Tothova, Z., Hegde, M., Smith, I., Sullender, M., Ebert, B.L., Xavier, R.J., and Root, D.E. (2014). Rational design of highly active sgRNAs for CRISPR-Cas9–mediated gene inactivation. Nature Biotechnology *32*, 1262–1267.

14. Dyson, N., Howley, P., Munger, K., and Harlow, E. (1989). The human papilloma virus-16 E7 oncoprotein is able to bind to the retinoblastoma gene product. Science *243*, 934.

15. Fay, D.S., and Han, M. (2000). The synthetic multivulval genes of C. elegans: functional redundancy, Ras-antagonism, and cell fate determination. Genesis *26*, 279–284.

16. Forristal, C., Henley, S.A., MacDonald, J.I., Bush, J.R., Ort, C., Passos, D.T., Talluri, S., Ishak, C.A., Thwaites, M.J., Norley, C.J., et al. (2014). Loss of the Mammalian DREAM Complex Deregulates Chondrocyte Proliferation. Mol. Cell. Biol. *34*, 2221.

17. Friend, S.H., Bernards, R., Rogelj, S., Weinberg, R.A., Rapaport, J.M., Albert, D.M., and Dryja, T.P. (1986). A human DNA segment with properties of the gene that predisposes to retinoblastoma and osteosarcoma. Nature *323*, 643–646.

18. Gaubatz, S., Lindeman, G.J., Ishida, S., Jakoi, L., Nevins, J.R., Livingston, D.M., and Rempel, R.E. (2000). E2F4 and E2F5 Play an Essential Role in Pocket Protein–Mediated G1 Control. Molecular Cell *6*, 729–735.

19. Georlette, D., Ahn, S., MacAlpine, D.M., Cheung, E., Lewis, P.W., Beall, E.L., Bell, S.P., Speed, T., Manak, J.R., and Botchan, M.R. (2007). Genomic profiling and expression studies reveal both positive and negative activities for the Drosophila Myb–MuvB/dREAM complex in proliferating cells. Genes & Development *21*, 2880–2896.

20. Guiley, K.Z., Liban, T.J., Felthousen, J.G., Ramanan, P., Litovchick, L., and Rubin, S.M. (2015). Structural mechanisms of DREAM complex assembly and regulation. Genes & Development *29*, 961–974.

21. Guiley, K.Z., Iness, A.N., Saini, S., Tripathi, S., Lipsick, J.S., Litovchick, L., and Rubin, S.M. (2018). Structural mechanism of Myb–MuvB assembly. Proc Natl Acad Sci USA *115*, 10016.

22. Harrison, M.M., Ceol, C.J., Lu, X., and Horvitz, H.R. (2006). Some C. elegans class B synthetic multivulva proteins encode a conserved LIN-35 Rb-containing complex distinct from a NuRD-like complex. Proc Natl Acad Sci USA *103*, 16782.

23. Helt, A.-M., and Galloway, D.A. (2003). Mechanisms by which DNA tumor virus oncoproteins target the Rb family of pocket proteins. Carcinogenesis *24*, 159–169.

24. Henley, S.A., and Dick, F.A. (2012). The retinoblastoma family of proteins and their regulatory functions in the mammalian cell division cycle. Cell Division *7*, 10.

25. Hiebert, S.W., Chellappan, S.P., Horowitz, J.M., and Nevins, J.R. (1992). The interaction of RB with E2F coincides with an inhibition of the transcriptional activity of E2F. Genes & Development *6*, 177–185.

26. Himpel, S., Tegge, W., Frank, R., Leder, S., Joost, H.-G., and Becker, W. (2000). Specificity Determinants of Substrate Recognition by the Protein Kinase DYRK1A. Journal of Biological Chemistry *275*, 2431–2438.

27. Hsu, P.D., Scott, D.A., Weinstein, J.A., Ran, F.A., Konermann, S., Agarwala, V., Li, Y., Fine, E.J., Wu, X., Shalem, O., et al. (2013). DNA targeting specificity of RNA-guided Cas9 nucleases. Nature Biotechnology *31*, 827–832.

28. Hurford, R.K., Cobrinik, D., Lee, M.H., and Dyson, N. (1997). pRB and p107/p130 are required for the regulated expression of different sets of E2F responsive genes. Genes & Development *11*, 1447–1463.

29. Iness, A.N., and Litovchick, L. (2018a). MuvB: A Key to Cell Cycle Control in Ovarian Cancer. Frontiers in Oncology *8*, 223.

30. Iness, A.N., Felthousen, J., Ananthapadmanabhan, V., Sesay, F., Saini, S., Guiley, K.Z., Rubin, S.M., Dozmorov, M., and Litovchick, L. (2019). The cell cycle regulatory DREAM complex is disrupted by high expression of oncogenic B-Myb. Oncogene *38*, 1080.

31. Jacks, T., Fazeli, A., Schmitt, E.M., Bronson, R.T., Goodell, M.A., and Weinberg, R.A. (1992). Effects of an Rb mutation in the mouse. Nature *359*, 295–300.

32. Jacobi, A.M., Rettig, G.R., Turk, R., Collingwood, M.A., Zeiner, S.A., Quadros, R.M., Harms, D.W., Bonthuis, P.J., Gregg, C., Ohtsuka, M., et al. (2017). Simplified CRISPR tools for efficient

genome editing and streamlined protocols for their delivery into mammalian cells and mouse zygotes. Methods *121–122*, 16–28.

33. Jones, R.E., Wegrzyn, R.J., Patrick, D.R., Balishin, N.L., Vuocolo, G.A., Riemen, M.W., Defeo-Jones, D., Garsky, V.M., Heimbrook, D.C., and Oliff, A. (1990). Identification of HPV-16 E7 peptides that are potent antagonists of E7 binding to the retinoblastoma suppressor protein. Journal of Biological Chemistry *265*, 12782–12785.

34. Jones, R.E., Heimbrook, D.C., Huber, H.E., Wegrzyn, R.J., Rotberg, N.S., Stauffer, K.J., Lumma, P.K., Garsky, V.M., and Oliff, A. (1992). Specific N-methylations of HPV-16 E7 peptides alter binding to the retinoblastoma suppressor protein. Journal of Biological Chemistry *267*, 908–912.

35. Knudsen, K.E., Booth, D., Naderi, S., Sever-Chroneos, Z., Fribourg, A.F., Hunton, I.C., Feramisco, J.R., Wang, J.Y., and Knudsen, E.S. (2000). RB-dependent S-phase response to DNA damage. Mol Cell Biol *20*, 7751–7763.

36. Korenjak, M., Taylor-Harding, B., Binné, U.K., Satterlee, J.S., Stevaux, O., Aasland, R., White-Cooper, H., Dyson, N., and Brehm, A. (2004). Native E2F/RBF Complexes Contain Myb-Interacting Proteins and Repress Transcription of Developmentally Controlled E2F Target Genes. Cell *119*, 181–193.

37. Kunstyr, I., and Leuenberger, H.W. (1975). Gerontological Data of C57BL/6J Mice. I. Sex Differences in Survival Curves1. Journal of Gerontology *30*, 157–162.

38. Lee, E.Y.-H.P., Chang, C.-Y., Hu, N., Wang, Y.-C.J., Lai, C.-C., Herrup, K., Lee, W.-H., and Bradley, A. (1992). Mice deficient for Rb are nonviable and show defects in neurogenesis and haematopoiesis. Nature *359*, 288–294.

39. Lee, J.-O., Russo, A.A., and Pavletich, N.P. (1998). Structure of the retinoblastoma tumour-suppressor pocket domain bound to a peptide from HPV E7. Nature *391*, 859–865.

40. Lee, M.H., Williams, B.O., Mulligan, G., Mukai, S., Bronson, R.T., Dyson, N., Harlow, E., and Jacks, T. (1996). Targeted disruption of p107: functional overlap between p107 and Rb. Genes & Development *10*, 1621–1632.

41. Lee, W., Bookstein, R., Hong, F., Young, L., Shew, J., and Lee, E. (1987). Human retinoblastoma susceptibility gene: cloning, identification, and sequence. Science *235*, 1394.

42. Lewis, P.W., Beall, E.L., Fleischer, T.C., Georlette, D., Link, A.J., and Botchan, M.R. (2004). Identification of a Drosophila Myb-E2F2/RBF transcriptional repressor complex. Genes & Development *18*, 2929–2940.

43. Liban, T.J., Thwaites, M.J., Dick, F.A., and Rubin, S.M. (2016). Structural Conservation and E2F Binding Specificity within the Retinoblastoma Pocket Protein Family. Journal of Molecular Biology *428*, 3960–3971.

44. Lin, D., Fiscella, M., O'Connor, P.M., Jackman, J., Chen, M., Luo, L.L., Sala, A., Travali, S., Appella, E., and Mercer, W.E. (1994). Constitutive expression of B-myb can bypass p53-induced Waf1/Cip1-mediated G1 arrest. Proc Natl Acad Sci U S A *91*, 10079–10083.

45. Litovchick, L., Sadasivam, S., Florens, L., Zhu, X., Swanson, S.K., Velmurugan, S., Chen, R., Washburn, M.P., Liu, X.S., and DeCaprio, J.A. (2007). Evolutionarily Conserved Multisubunit RBL2/p130 and E2F4 Protein Complex Represses Human Cell Cycle-Dependent Genes in Quiescence. Molecular Cell *26*, 539–551.

46. Litovchick, L., Florens, L.A., Swanson, S.K., Washburn, M.P., and DeCaprio, J.A. (2011). DYRK1A protein kinase promotes quiescence and senescence through DREAM complex assembly. Genes & Development *25*, 801–813.

47. MacDonald, J., Ramos-Valdes, Y., Perampalam, P., Litovchick, L., DiMattia, G.E., and Dick, F.A. (2017). A Systematic Analysis of Negative Growth Control Implicates the DREAM Complex in Cancer Cell Dormancy. Mol Cancer Res *15*, 371.

48. Mages, C.F., Wintsche, A., Bernhart, S.H., and Müller, G.A. (2017). The DREAM complex through its subunit Lin37 cooperates with Rb to initiate quiescence. ELife *6*, e26876.

49. Malumbres, M., and Barbacid, M. (2009). Cell cycle, CDKs and cancer: a changing paradigm. Nature Reviews Cancer *9*, 153–166.

50. Mannefeld, M., Klassen, E., and Gaubatz, S. (2009). B-MYB Is Required for Recovery from the DNA Damage–Induced G_2 Checkpoint in p53 Mutant Cells. Cancer Res *69*, 4073.

51. Mason, D.X., Jackson, T.J., and Lin, A.W. (2004). Molecular signature of oncogenic ras-induced senescence. Oncogene *23*, 9238–9246.

52. Mulligan, G.J., Wong, J., and Jacks, T. (1998a). p130 is dispensable in peripheral T lymphocytes: evidence for functional compensation by p107 and pRB. Mol Cell Biol *18*, 206–220.

53. Mulligan, G.J., Wong, J., and Jacks, T. (1998b). p130 is dispensable in peripheral T lymphocytes: evidence for functional compensation by p107 and pRB. Mol Cell Biol *18*, 206–220.

54. Musa, J., Aynaud, M.-M., Mirabeau, O., Delattre, O., and Grünewald, T.G. (2017). MYBL2 (B-Myb): a central regulator of cell proliferation, cell survival and differentiation involved in tumorigenesis. Cell Death & Disease *8*, e2895–e2895.

55. Nor Rashid, N., Yusof, R., and Watson, R.J. (2011). Disruption of repressive p130–DREAM complexes by human papillomavirus 16 E6/E7 oncoproteins is required for cell-cycle progression in cervical cancer cells (Microbiology Society).

56. Paternot, S., Dumont, J.E., and Roger, P.P. (2006). Differential Utilization of Cyclin D1 and Cyclin D3 in the Distinct Mitogenic Stimulations by Growth Factors and TSH of Human Thyrocytes in Primary Culture. Molecular Endocrinology *20*, 3279–3292.

57. Pilkinton, M., Sandoval, R., and Colamonici, O.R. (2007). Mammalian Mip/LIN-9 interacts with either the p107, p130/E2F4 repressor complex or B-Myb in a cell cycle-phase-dependent context distinct from the Drosophila dREAM complex. Oncogene *26*, 7535–7543.

58. Qin, X.Q., Chittenden, T., Livingston, D.M., and Kaelin, W.G. (1992). Identification of a growth suppression domain within the retinoblastoma gene product. Genes & Development *6*, 953–964.

59. Reichert, N., Wurster, S., Ulrich, T., Schmitt, K., Hauser, S., Probst, L., Götz, R., Ceteci, F., Moll, R., Rapp, U., et al. (2010). Lin9, a Subunit of the Mammalian DREAM Complex, Is Essential for Embryonic Development, for Survival of Adult Mice, and for Tumor Suppression. Mol. Cell. Biol. *30*, 2896.

60. Rubin, S.M., Gall, A.-L., Zheng, N., and Pavletich, N.P. (2005). Structure of the Rb C-Terminal Domain Bound to E2F1-DP1: A Mechanism for Phosphorylation-Induced E2F Release. Cell *123*, 1093–1106.

61. Sadasivam, S., and DeCaprio, J.A. (2013). The DREAM complex: master coordinator of cell cycle-dependent gene expression. Nature Reviews Cancer *13*, 585.

62. Sadasivam, S., Duan, S., and DeCaprio, J.A. (2012). The MuvB complex sequentially recruits B-Myb and FoxM1 to promote mitotic gene expression. Genes & Development *26*, 474–489.

63. Schafer, K.A. (1998). The Cell Cycle: A Review. Vet Pathol *35*, 461–478.

64. Schmit, F., Korenjak, M., Mannefeld, M., Schmitt, K., Franke, C., von Eyss, B., Gagrica, S., Hanel, F., Brehm, A., and Gaubatz, S. (2007). LINC, a Human Complex That is Related to pRB-Containing Complexes in Invertebrates Regulates the Expression of G2/M Genes. Cell Cycle *6*, 1903–1913.

65. Serrano, M., Lin, A.W., McCurrach, M.E., Beach, D., and Lowe, S.W. (1997). Oncogenic ras Provokes Premature Cell Senescence Associated with Accumulation of p53 and p16INK4a. Cell *88*, 593–602.

66. Trimarchi, J.M., and Lees, J.A. (2002). Sibling rivalry in the E2F family. Nature Reviews Molecular Cell Biology *3*, 11–20.

67. Wells, J., Boyd, K.E., Fry, C.J., Bartley, S.M., and Farnham, P.J. (2000). Target Gene Specificity of E2F and Pocket Protein Family Members in Living Cells. Mol. Cell. Biol. *20*, 5797.

68. Whyte, P., Buchkovich, K.J., Horowitz, J.M., Friend, S.H., Raybuck, M., Weinberg, R.A., and Harlow, E. (1988). Association between an oncogene and an anti-oncogene: the adenovirus E1A proteins bind to the retinoblastoma gene product. Nature *334*, 124–129.

69. Woo, M.S., Sánchez, I., and Dynlacht, B.D. (1997). p130 and p107 use a conserved domain to inhibit cellular cyclin-dependent kinase activity. Mol Cell Biol *17*, 3566–3579.

70. Zhu, W., Giangrande, P.H., and Nevins, J.R. (2004). E2Fs link the control of G1/S and G2/M transcription. EMBO J *23*, 4615–4626.